

# On behaviour and scaling of small repeating earthquakes in rate and state fault models

Ting Chen<sup>1</sup> and Nadia Lapusta<sup>2,3</sup>

<sup>1</sup>*Division of Earth and Environmental Sciences, Los Alamos National Laboratory, Los Alamos, NM 87545, USA. E-mail: tchen@lanl.gov*

<sup>2</sup>*Seismological Laboratory, California Institute of Technology, Pasadena, CA 91125, USA*

<sup>3</sup>*Department of Mechanical and Civil Engineering, California Institute of Technology, Pasadena, CA 91125, USA*

Accepted 2019 June 6. Received 2018 September 29; in original form 2019 May 28

## SUMMARY

With abundant seismic data for small repeating earthquakes, it is important to construct a dynamic model that can explain various aspects of related observations. In this work, we study small repeating earthquakes on a fault governed by rate- and state-dependent friction laws. The earthquakes occur on a velocity-weakening patch surrounded by a much larger velocity-strengthening region. The whole fault is subject to long-term tectonic loading. The model with a circular patch and the aging form of rate- and state-dependent friction laws has been shown to reproduce the scaling of recurrence time versus seismic moment for small repeating earthquakes in a previous study. Here we investigate the behaviour of small repeating earthquakes in related models under different scenarios, including several forms of the state evolution equations in rate- and state-dependent friction laws, rectangular velocity-weakening patch geometries, quasi-dynamic versus fully dynamic representation of inertial effects and 2-D versus 3-D simulations. We find that the simulated scalings between the recurrence time and seismic moment for these different scenarios is similar while differences do exist. We propose a theoretical consideration for the scaling between the recurrence time and seismic moment of small repeating earthquakes. For patch radii smaller than or comparable to the full nucleation size, the scaling is explained by the increase of seismic to aseismic slip ratio with magnitude. For patch radii larger than the full nucleation size, the scaling is explained by the model in which the recurrence time is determined by the earthquake nucleation time, which is in turn determined by the time for aseismic slip to penetrate the distance of the full nucleation size into the patch. The obtained theoretical insight is used to find the combinations of fault properties that allow the model to fit the observed scaling and range of the seismic moment and recurrence time.

**Key words:** Earthquake dynamics; Rheology and friction of fault zones; Seismicity and tectonics; Dynamics and mechanics of faulting; Mechanics, theory, and modelling.

## 1 INTRODUCTION

Repeating earthquakes occur in the same location, and presumably rupture the same patch of the fault in a similar way, to produce nearly identical seismic signals. The short recurrence times and known locations of small repeating earthquakes enable abundant and detailed seismic observations (e.g. Vidale *et al.* 1994; Nadeau & Johnson 1998; Igarashi *et al.* 2003), and thus provide an excellent opportunity to study the earthquake source and fault properties. Studies of repeating earthquakes have been used to investigate an increasingly richer array of problems, including fault creeping velocities, post-seismic slip, earthquake interaction and stress drops (Vidale *et al.* 1994; Nadeau & Johnson 1998; Schaff *et al.* 1998;

Peng *et al.* 2005; Chen *et al.* 2007; Dreger *et al.* 2007; Chen *et al.* 2010; Lui & Lapusta 2016).

One of the most interesting observations about small repeating earthquakes is the scaling between the recurrence time  $T$  and seismic moment  $M_0$  as  $T \propto M_0^{0.17}$  (Nadeau & Johnson 1998; Chen *et al.* 2007). This observed scaling is different from that of a simple conceptual model with circular ruptures, constant stress drop and seismic slip equalling to plate velocity times recurrence time, which would result in a relationship of  $T \propto M_0^{1/3}$ . Various explanations for this discrepancy have been proposed: the magnitude dependence of stress drops (Nadeau & Johnson 1998), location of small repeating earthquakes at the boundary between much larger creeping and locked regions (Sammis & Rice 2001) and partial aseismic slip due to strain hardening friction (Beeler *et al.* 2001).

Chen & Lapusta (2009) conducted fully dynamic simulations of small repeating earthquakes in a model with a small circular patch governed by standard rate-and-state velocity-weakening friction surrounded by a much larger velocity-strengthening region, using the aging form of the state variable evolution. Their model results in repeating earthquakes with typical stress drops of 1–10 MPa and sizes comparable with observations, and reproduces the observed scaling between the seismic moment and recurrence time. Chen & Lapusta (2009) attributed the simulated scaling to the fact that the seismic to aseismic slip ratio increases with the seismic moment. To match the absolute values of the observed recurrence times for the repeaters on the creeping section of the San Andreas fault (SAF), the model needs to use much lower values of the loading creeping rate,  $4.5 \text{ mm yr}^{-1}$ , than the average creeping rate of  $23 \text{ mm yr}^{-1}$  inferred for the segment (Lisowski & Prescott 1981; Murray *et al.* 2001; Titus *et al.* 2006), although the available data allow for significant uncertainty regarding the creeping rate and its spatial distribution (Jolivet *et al.* 2015). The creeping rate influencing repeating earthquakes can be further reduced by the potential presence of several creeping strands (Zoback *et al.* 2010, 2011). The model of Chen & Lapusta (2009) has also been used to study the post-seismic response of small repeating earthquakes to a nearby large event (Chen *et al.* 2010). By varying the loading velocity to simulate the post-seismic creep effect, the model successfully explains the observed temporal variation in seismic moment and recurrence time of small repeating earthquakes near Parkfield after the 2004 M6 Parkfield earthquake. Using a quasi-dynamic approximation, Cattania & Segall (2019) have further investigated the behaviour of repeating earthquakes in the model numerically and derived theoretical estimates for the recurrence time based on energy balance concepts.

To allow such models to produce higher stress drops, as observed for some repeaters (i.e. the SF and LA repeaters) on the San Andreas fault (Dreger *et al.* 2007; Abercrombie 2014), they have been extended to include either enhanced dynamic weakening during seismic slip or an elevated normal stress at the seismogenic patch (Lui & Lapusta 2018). Such augmented modelling can simultaneously reproduce the higher observed stress drops for the SF and LA repeaters, their interaction timing prior to 2004, their long (for the stress drop) recurrence times, their moments, their variability and the overall scaling of the repeating sequences on the creeping segment, using the loading velocity of  $23 \text{ mm yr}^{-1}$ .

Here we investigate the behaviour of small repeating earthquakes on a rate and state fault under different modelling assumptions, including several forms of the state variable evolution, quasi-dynamic versus fully dynamic formulations, different shapes of the seismogenic region and 2-D versus 3-D models. We propose a theoretical model to understand the simulated results in terms of the scaling between the recurrence time and seismic moment and determine the parameter ranges that can reproduce the observed properties of the repeaters.

## 2 MODEL FOR SMALL REPEATING EARTHQUAKES

Our model for small repeating earthquakes is based on the one in Chen & Lapusta (2009) (Fig. 1). We simulate earthquakes on a fault governed by laboratory-derived rate and state friction laws (Dieterich 1979, 1981; Ruina 1983; Marone 1998; Dieterich 2007

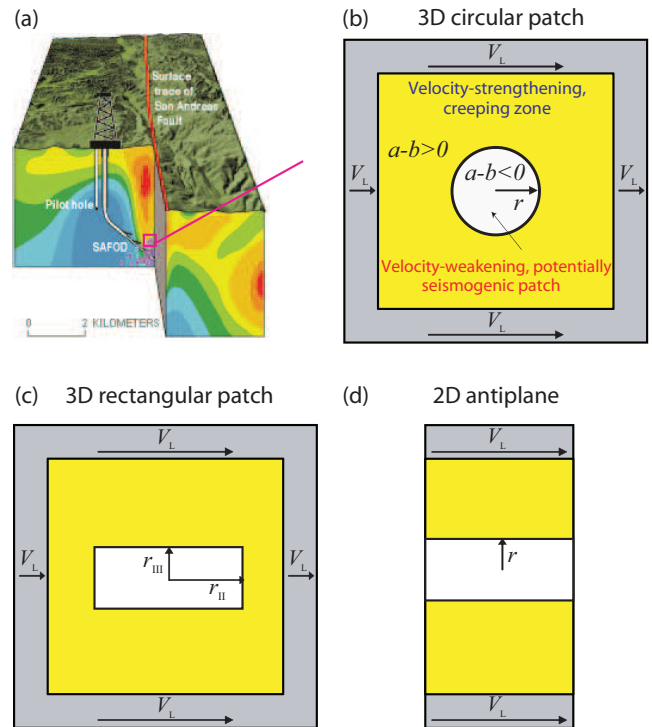


**Figure 1.** Schematics of the models. To simulate repeating earthquakes, such as (a) the target events of SAFOD drilling project (image courtesy of U. S. Geological Survey), we consider a small segment of the fault embedded into an elastic medium and governed by rate and state friction laws. On the fault, a velocity-weakening, potentially seismogenic, patch is surrounded by a creeping, velocity-strengthening zone. 3-D models with a (b) circular and (c) rectangular patches as well as (d) a 2-D antiplane model are studied.

and references therein). Rate and state friction laws have been successfully applied to modelling of various fault slip phenomena (Dieterich 2007 and references therein). For constant in time normal stress  $\sigma$ , shear resistance  $\tau$  obeying rate and state friction laws is written as:

$$\tau = \sigma [f_0 + a \ln(V/V_0) + b \ln(V_0\theta/L)], \quad (1)$$

$$\tau_{ss} = \sigma [f_0 + (a - b) \ln(V/V_0)], \quad (2)$$

where  $V$  is slip velocity,  $\theta$  is a state variable,  $L$  is the characteristic slip distance,  $a$  and  $b$  are rate-and-state parameters,  $V_0$  and  $f_0$  are the reference slip velocity and friction coefficient, respectively, and  $\tau_{ss}$  is steady-state shear resistance. Different forms of the state evolution equation have been proposed based on laboratory experiments (e.g. Ruina 1983; Kato & Tullis 2001; Dieterich 2007). Which formulation best represents laboratory experiments is a question of active studies (Bhattacharya *et al.* 2015, 2017). Here we investigate models with the following forms:

$$d\theta/dt = 1 - V\theta/L \quad (\text{the aging form}), \quad (3)$$

$$d\theta/dt = -V\theta/L \ln(V\theta/L) \quad (\text{the slip form}), \quad (4)$$

$$d\theta/dt = \exp(-V/V_c) - V\theta/L \ln(V\theta/L) \quad (\text{the composite form}), \quad (5)$$

and

$$d\theta/dt = \begin{cases} 1 - V\theta/L, & \text{when } V\theta/L < 1, \\ -V\theta/L \ln(V\theta/L), & \text{when } V\theta/L \geq 1 \end{cases}$$

(the combined form). (6)

We refer to the fault regions with  $a - b > 0$  as being velocity strengthening, and  $a - b < 0$  as being velocity weakening. Velocity-strengthening fault regions tend to stably slip (creep) under loading, and velocity-weakening fault regions are able to produce seismic events when they are larger than the nucleation zone size  $2h^*$  (Rice & Ruina 1983; Dieterich 1992; Rice 1993; Rubin & Ampuero 2005). Several estimates for the nucleation half-length  $h^*$  with different dependence on  $b$  and  $(b - a)$  have been proposed, each based on different assumptions. We denote them as  $h_b^*$ ,  $h_{b-a}^*$  and  $h_{RA}^*$  in reference to quantities introduced by Dieterich (1992), Rice (1993) and Rubin & Ampuero (2005) respectively:

$$h_b^* = \frac{\hat{\mu}L}{\sigma b}, \quad (7)$$

$$h_{b-a}^* = \frac{\hat{\mu}L}{\pi\sigma(b-a)}, \quad (8)$$

$$h_{RA}^* = \frac{\hat{\mu}Lb}{\pi\sigma(b-a)^2}, \quad (9)$$

where  $\hat{\mu} = \mu$  for antiplane sliding and  $\hat{\mu} = \mu/(1 - \nu)$  for inplane sliding with  $\nu$  being the Poisson's ratio. The 3-D analogue of  $h_{RA}^*$ , which is larger than that in eq. (9) for 2-D antiplane case by a factor of  $\pi^2/4$ , is in agreement with numerical simulations with the aging form of state-variable evolutions (Chen & Lapusta 2009). In part, our simulations explore the relation of these theoretical estimates to the nucleation sizes numerically obtained in our modelling.

In our model, a planar fault is embedded in an elastic medium with the following properties: shear modulus  $\mu = 30$  GPa, Poisson's ratio  $\nu = 0.25$ , shear wave speed  $c_s = 3$  km s<sup>-1</sup>. On the fault, a potentially seismogenic patch is surrounded by a larger creeping zone. The patch has velocity-weakening properties,  $a - b < 0$ , and the surrounding region has velocity-strengthening properties,  $a - b > 0$ . A similar model setup has also been used in other studies (e.g. Kato 2012). The values of  $a$  and  $b$  of the velocity-strengthening region are set to be equal to the values of  $b$  and  $a$  of the velocity-weakening region, respectively; thus we only mention the values of  $a$  and  $b$  in the velocity-weakening region in the following. Long-term slip velocity  $V_L$  is imposed outside the velocity-strengthening zone to model steady creep of the surrounding fault area. The spontaneous slip history of the fault is solved using the methodology of Lapusta & Liu (2009), which can fully resolve all aspects of seismic and aseismic behaviour. In our simulations, we use the following values from Chen & Lapusta (2009): effective normal stress  $\sigma = 50$  MPa, reference friction coefficient  $f_0 = 0.6$ , reference slip velocity  $V_0 = 1$   $\mu$ m s<sup>-1</sup>, characteristic slip  $L = 160$   $\mu$ m and loading velocity  $V_L = 23$  mm a<sup>-1</sup> (Nadeau & Johnson 1998). We define seismic slip as the slip accumulated with slip velocities larger than  $0.1$  m s<sup>-1</sup>.

### 3 RESPONSE OF MODELS WITH DIFFERENT STATE EVOLUTION LAWS

Chen & Lapusta (2009) used the aging form in their simulations of small repeating earthquakes. Here we study the effect of other state evolution forms (eqs 4–6) on the behaviour of small repeating earthquakes.

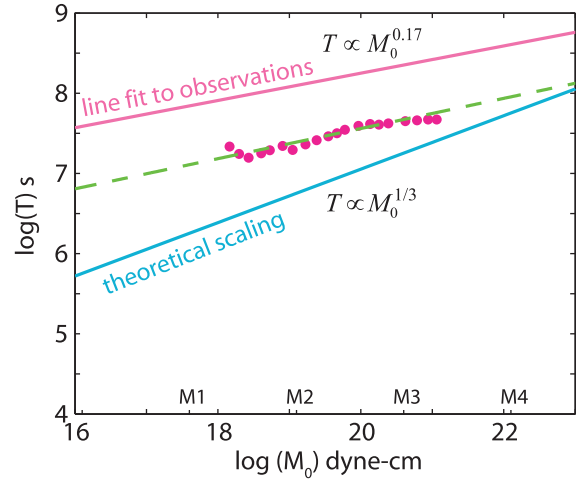


**Figure 2.** Simulated scaling of the recurrence time  $T$  with seismic moment  $M_0$  for the slip form of state evolution ( $b = 0.023$ ,  $b - a = 0.008$ ). Sequences of repeating events with different moments and recurrence times are obtained by varying the radius of the VW patch. The simulated scaling for the slip form in this study (dots) is similar to that for the aging form (green dashed line from Chen & Lapusta 2009). The simulated scaling exponent is similar to the observations (magenta line, from Nadeau & Johnson 1998), and different from the prediction of a simple theoretical model with constant stress drop and no aseismic slip (blue line). The results for  $V_L = 23$  mm a<sup>-1</sup> are plotted; as shown in Chen & Lapusta (2009), our simulations can match observations for  $V_L = 4.5$  mm a<sup>-1</sup>.

Let us first consider the response of models with the slip form. We set  $a = 0.015$  and  $b = 0.023$ , and obtain different magnitudes of repeating earthquakes by varying the velocity-weakening patch radius  $r$ . We choose  $(b - a)$  of 0.008, which is larger than the typical value of 0.004 as used in Chen & Lapusta (2009), because the nucleation half-length is smaller for larger  $(b - a)$  and thus it is easier to study a larger range of  $r/h^*$ . In Chen & Lapusta (2009), the simulated range of  $r/h^*$  is about 1 to 4 for  $a = 0.015$ ,  $b - a = 0.004$ . Here we extend the range of  $r/h^*$  to about 1 to 11. The simulated earthquakes show a similar exponent of the scaling between the recurrence time and seismic moment to that with the aging form (Fig. 2). The absolute value of the simulated recurrence time is lower than the observations. As shown in Chen & Lapusta (2009), we can match the absolute values of the observed recurrence time while maintaining the scaling exponent by using  $V_L = 4.5$  mm a<sup>-1</sup> instead of  $V_L = 23$  mm a<sup>-1</sup>. Here, we use 23 mm a<sup>-1</sup> for numerical convenience (faster loading results in shorter interseismic time).

We also study different sets of parameters  $a$  and  $b$ . In general, the simulated overall scaling of recurrence time and seismic moment with different parameters  $a$ ,  $b$  is similar to the simulated scaling with the aging form, which is flatter than the theoretical scaling  $T \propto M_0^{1/3}$  (Fig. 3b). The individual scalings for different sets of parameters  $a$  and  $b$ , however, seem to show some difference. In particular, simulation results with smaller  $(b - a)$  of 0.002 and 0.004, especially with  $(b - a)$  of 0.002, show steeper scaling than the observed one. This is likely due to the fact that for  $(b - a)$  of 0.002 and 0.004, only relatively small patch sizes relative to the nucleation length are studied due to computational limitation. The simulated range of  $r/h^*$  for  $(b - a)$  of 0.002, 0.004, 0.008 and 0.02 is about 1 to 3, 1 to 6, 1 to 11 and 1 to 17, respectively. As discussed in section 8, the scaling between the recurrence time and seismic moment is predicted (theoretically) to be steeper for relatively small ratios of the patch size to nucleation size. Note that, for the same  $(b - a)$ , the simulated recurrence time and seismic moment are

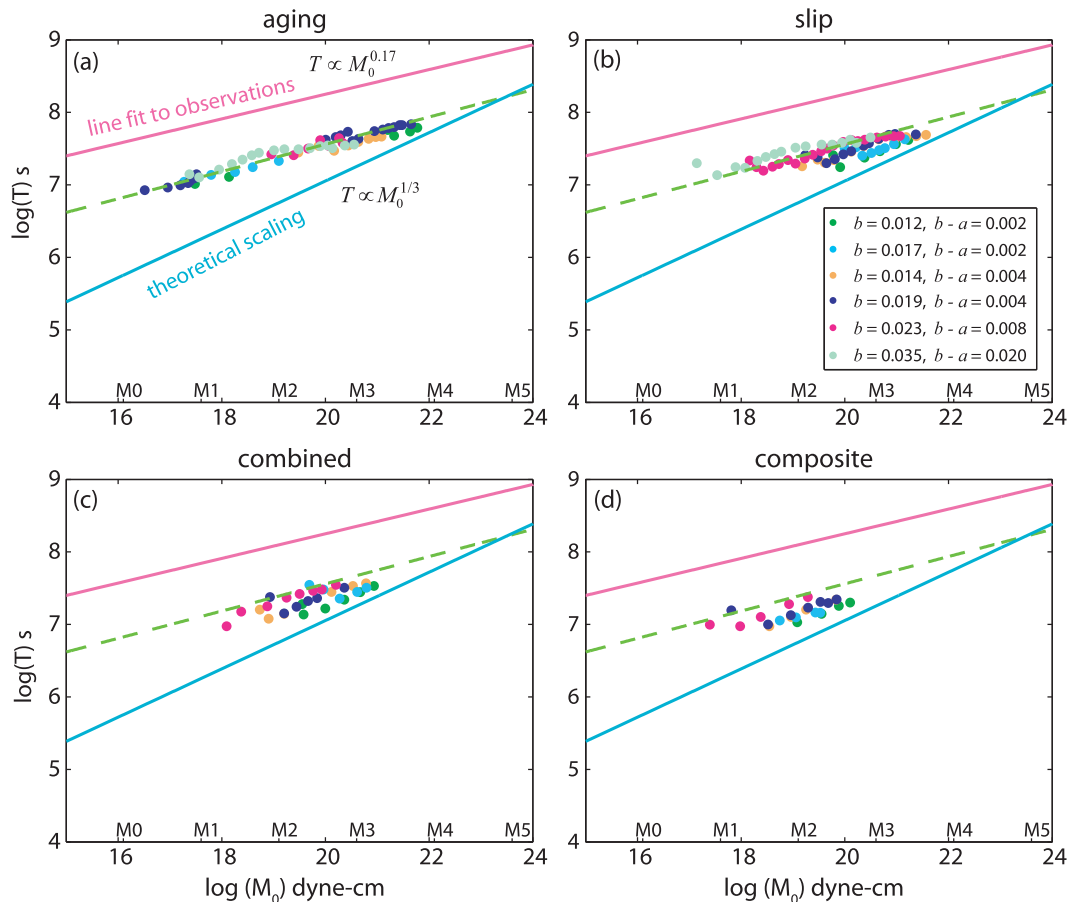


**Figure 3.** Simulated scaling of the recurrence time with seismic moment for different state evolution forms: (a) aging form (mostly adapted from Chen & Lapusta (2009), except for the simulations with  $a = 0.015$ ,  $b = 0.035$ ), (b) slip form, (c) combined form and (d) composite form. Different colours represent simulations with different  $a$  and  $b$ . The overall scaling exponents with the four different state evolution forms are all similar to the observations. Some individual scalings with certain  $a$  and  $b$ , for example,  $b - a = 0.002$  and  $b - a = 0.004$  for the slip form, combined form, and composite form, seem to have larger exponents. This is because for these  $a$  and  $b$ , only relatively small patch sizes are studied due to computational limitations. Please see the text for more discussion. The lines have the same meaning as in Fig. 2.

almost the same. The absolute level of recurrence time increases with larger  $(b - a)$ . For the sets of parameters  $a$ ,  $b$  we studied, the absolute levels of recurrence time for simulations with the slip form (Fig. 3b) show larger variations than that with the aging form (Fig. 3a).

We have also studied the combined form (Fig. 3c) and composite form (Fig. 3d). The simulated overall scaling for both the combined form and composite form are similar to that with the aging and slip form. The scaling for smaller  $(b - a)$  is steeper than the observed one due to limited simulated range of  $r/h^*$ . The magnitudes of the simulated smallest events for different values of  $a$  and  $b$  with the combined form are about the same as those with the slip form, while the simulated events with the composite form are generally smaller than that with the slip form. This is because the nucleation length for the composite form is generally smaller than that for the slip form or combined form as discussed in Section 7, and thus the patch sizes needed to produce seismic events are generally smaller, resulting in smaller seismic moments.

Note that for the aging form (Fig. 3a), the resulting  $T$  and  $M_0$  cluster around a single line. For the other forms (Figs 3b–d), the simulations for individual  $a$  and  $b$  combinations displace with respect to each other. For the slip, combined and composite forms, the simulated levels of  $T$  versus  $M_0$  seem to depend only on  $(b - a)$ .

Simulations with the aging form produce earthquakes that rupture only a small central portion of the velocity-weakening patch when the patch size is comparable to the nucleation size and  $(b - a)$  is relatively small (0.002 and 0.004) (Chen & Lapusta 2009). This type of event has been proposed to explain the increased seismic moment with decreased recurrence time observed for postseismic response of small repeating earthquakes to 2004 M6 Parkfield earthquake (Chen *et al.* 2010). Simulations with the slip form, combined form or composite form, however, do not commonly produce events of this kind; the simulated patch behaviour sharply switches from being totally aseismic to rupturing the whole velocity-weakening patch. Yet it is possible that events that rupture only a part of the patch can be obtained with the slip, combined and composite forms, if the model includes heterogeneous patches or patches with a constitutive response that incorporates a stabilizing factor such as pore pressure decrease due to inelastic dilatancy (e.g. Segall & Rice 1995; Segall *et al.* 2010).

#### 4 CIRCULAR VERSUS RECTANGULAR PATCHES

In Chen & Lapusta (2009), the potentially seismogenic velocity-weakening region is assumed to be circular. Here we consider the

effect of a rectangular geometry, using the other parameters from the model of Chen & Lapusta (2009): the aging form of state evolution equation,  $a = 0.015$  and  $b = 0.019$  for the velocity-weakening region and  $a = 0.019$ ,  $b = 0.015$  for the velocity-strengthening region. The resulting 3-D estimate of the half nucleation size  $h_{RA}^*$  is about 90 m. In the rest of the section, we use  $h^*$  to denote the 3-D estimate of  $h_{RA}^*$  for simplicity. The rectangular velocity-weakening region has dimensions of  $2r_{II}$  and  $2r_{III}$  in the mode II and mode III directions, respectively (Fig. 1c). We study cases with different patch half-widths  $r_{III}$  of 40, 50, 60, 70, 80, 100 and 130 m, corresponding to  $r_{III}/h^*$  of 0.4, 0.6, 0.7, 0.8, 0.9, 1.1 and 1.4, respectively. For each  $r_{III}$ , we obtain different sizes of earthquakes by changing  $r_{II}$ .

We observe four types of slip patterns (Figs 4b, 5–7): periodic aseismic; seismic pattern I in which seismic events rupture only a part of the velocity-weakening patch and result in small magnitudes (Fig. 5); seismic pattern II in which seismic events rupture the whole velocity-weakening patch and have much larger magnitudes (Fig. 6) and non-characteristic in which different slip patterns occur in one sequence, and not in a repeating way (Fig. 7). As expected, events are more seismic when the patch size is larger. Seismic events of pattern I have also been observed with a circular patch (Chen & Lapusta 2009). Note that if both  $r_{II}$  and  $r_{III}$  are large enough compared with the nucleation half-length, seismic ruptures tend to start at one side of the patch while the centre of the patch is still locked (Fig. 6b). If  $r_{III}$  is a little smaller than the nucleation half-length, even though  $r_{II}$  is much larger than the nucleation half-length, aseismic slip creeps all the way into the centre of the patch, and seismic ruptures start from the centre (Fig. 6a). The non-characteristic pattern could be non-periodic seismic or non-periodic aseismic depending on the patch dimensions. Similar non-characteristic pattern has also been observed in some other studies (e.g. Hirose & Hirahara 2002).

Our studies show that the width and length of a velocity-weakening patch do compensate each other to some extent in terms of nucleation. The required size of  $r_{II}$  to produce seismic event is smaller for larger  $r_{III}$ . However, this is only valid for a certain range of  $r_{III}/h^*$ . For  $r_{III}$  small compared with the nucleation length ( $r_{III}/h^* \lesssim 0.4$ ), no seismic events are observed. Seismic events that rupture the whole velocity-weakening patch are only obtained for  $r_{III}$  close to or larger than the nucleation length ( $r_{III}/h^* \gtrsim 0.9$ ). Non-characteristic slip patterns are observed when  $r_{III}/h^*$  is smaller than 1 and  $r_{II}/h^*$  is large enough. We also expect non-repeating patterns when both  $r_{III}/h^*$  and  $r_{II}/h^*$  are large enough. This is because when one or both of the dimensions of the velocity-weakening patch get large compared with the nucleation length, more freedom exists for nucleation processes, resulting in different slip patterns in one sequence.

Based on the simulations we have done, we expect that the results would stay qualitatively similar if the values of  $r_{II}$  and  $r_{III}$  were switched. For example, since  $r_{II}/h^* \approx 5$  and  $r_{III}/h^* \approx 0.7$  results in non-characteristic events, we expect  $r_{II}/h^* \approx 0.7$  and  $r_{III}/h^* \approx 5$  to do the same. So all our conclusions should hold with  $r_{II}$  and  $r_{III}$  reversed.

Despite the increased complexity of the patch response in terms of the slip patterns compared to the circular patch, the qualitative behaviour in terms of partitioning into aseismic and seismic slip is similar and hence the simulated scaling between the recurrence time and seismic moment with the rectangular patch (Fig. 4a) is also similar to the results with a circular patch and to observations. Hence the observed repeating earthquakes may be occurring on patches of non-circular shape. Note that patches with elliptical shape were used to explain the temporal behaviour of tremors below the creeping section of the San Andreas Fault (Veedu & Barbot 2016).

## 5 QUASI-DYNAMIC VERSUS FULLY DYNAMIC SIMULATIONS

Quasi-dynamic approach has been widely used in earthquake simulation studies (e.g. Rice 1993; Ben-Zion & Rice 1995; Hori *et al.* 2004; Kato 2004; Hillers *et al.* 2006). Compared with the fully dynamic approach, quasi-dynamic approach ignores wave-mediated stress transfers, with computations becoming much simplified and less expensive. However, the quasi-dynamic approach can result in qualitative differences in the simulated results (Thomas *et al.* 2014). Here we compare fully dynamic simulations with quasi-dynamic simulations, with the same model as in Chen & Lapusta (2009).

Results with quasi-dynamic simulations and fully dynamic simulations show similar scaling between the recurrence time and seismic moment (Fig. 8). However, differences do exist in terms of the recurrence time, seismic moment, effective rupture size and maximum slip rate on the fault (Fig. 9). The 3-D analogue of the nucleation half-length  $h_{RA}^*$  in these simulations is about 90 m. The patch radii  $r$  of 106 and 124 m produce seismic pattern I slip that ruptures only a part of the patch, and  $r$  of 150, 200 and 300 m produce seismic pattern II slip that ruptures the whole velocity-weakening patch. The ratio of the maximum slip rate on the fault in fully dynamic and quasi-dynamic simulations increases with patch radius, and can be as high as 6 for  $r = 300$  m. The effective rupture size, defined as the radius of the seismically ruptured area, is larger for fully dynamic simulations, especially for seismic pattern I events. Larger slip rates and effective rupture sizes for fully dynamic simulations result in larger seismic moments and longer recurrence times than those of quasi-dynamic simulations for seismic pattern II events. For seismic pattern I events, the seismic moment of fully dynamic simulations is also higher than that of quasi-dynamic simulations, but the recurrence times are about the same, because seismic slip only contributes a very small part of the total slip in these cases.

Note that the rupture pattern for the two simulation approaches can be quite different. In the example shown in Fig. 10, fully dynamic simulations produce creep events (with slip velocity that does not reach the seismic limit of  $0.1 \text{ m s}^{-1}$ ) between large seismic event, while quasi-dynamic simulations do not show such creep events.

## 6 2-D VERSUS 3-D SIMULATIONS

2-D simulations require much less computation than 3-D simulations. So it is important to see if we can obtain the same scaling in 2-D simulations as in 3-D ones. We study an antiplane (mode III) 2-D case. The velocity-weakening patch turns into an infinite strip with width  $2r$  (Fig. 1d). The aging form of the state evolution equation is adopted, with the same parameters as in the 3-D simulations of Chen & Lapusta (2009).

Since the fault area is infinite in 2-D, the computation of seismic moment is not straightforward. We use two approaches. One is computing the seismic moment per unit length of the fault. The other one is interpreting 2-D simulation results in terms of a 3-D problem as in Lapusta & Rice (2003). The first approach results in a different scaling between the recurrence time and seismic moment from that of observation (Fig. 11a). If we use the second approach, the scaling becomes similar to the one in the 3-D simulation results (Fig. 11b).

Note that, unlike simulations with the 3-D model, simulations with the 2-D model do not produce seismic pattern I events that rupture only a part of the velocity-weakening patch, even though both 2-D and 3-D simulations use the aging form. This means that fault geometry affects the rupture pattern.

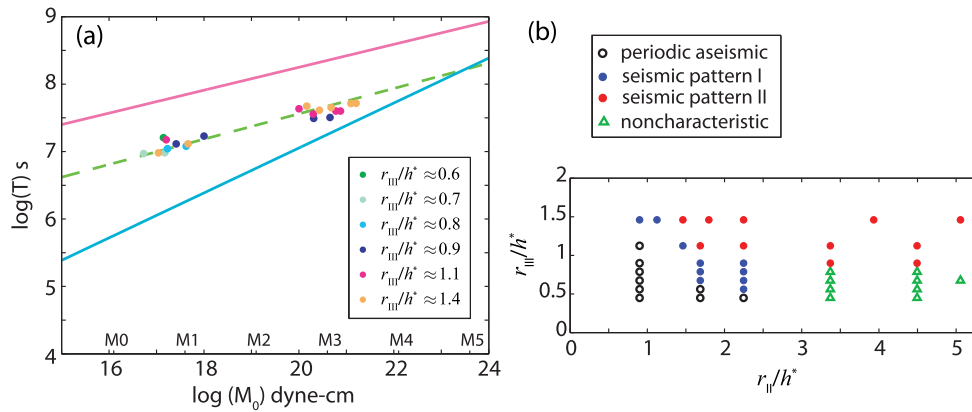


**Figure 4.** (a) Scaling of the recurrence time with seismic moment for simulations with a rectangular velocity-weakening patch. The aging form is used ( $a = 0.015$ ,  $b = 0.019$ ).  $h^*$  stands for the 3-D analogue of  $h_{RA}^*$ . Different colours represent simulations with different half widths  $r_{III}$  of the patch. For the same half width of the patch, the half length of the patch ( $r_{II}$ ) is varied to produce different sizes of events. The resulting overall scaling is similar to that with a circular patch. The lines have the same meaning as in Fig. 2. (b) Different slip patterns for different sizes of the rectangular patch. Note that the rectangular patch with  $r_{III}/h^*$  smaller than 1 is still able to produce seismic events for a certain range of  $r_{II}/h^*$ .

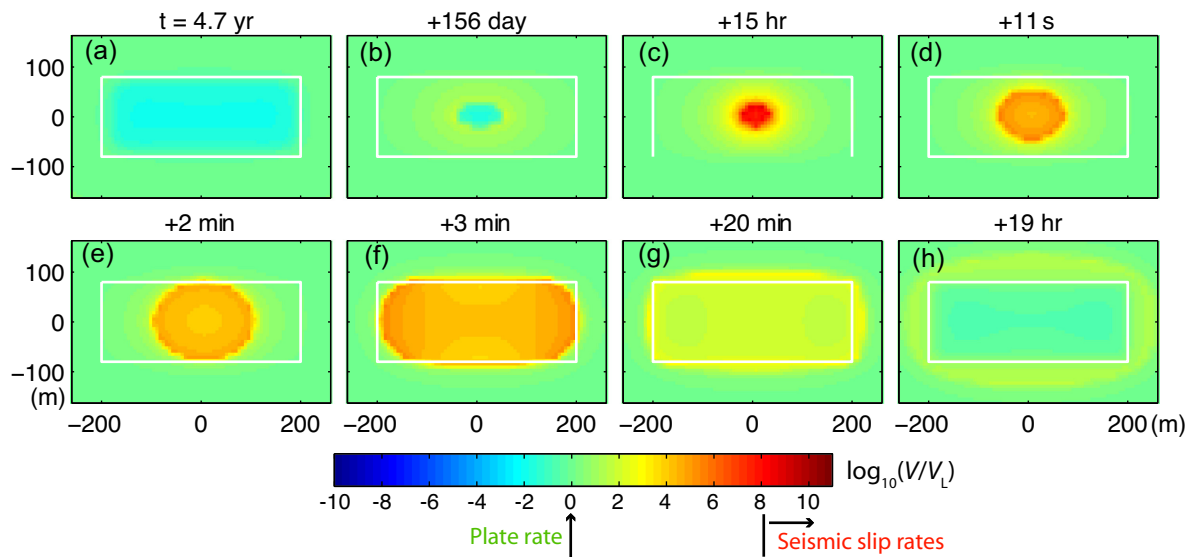


**Figure 5.** Example of an event of seismic pattern I with a rectangular patch ( $r_{III}/h^* = 0.9$ ,  $r_{II}/h^* = 2.2$ ). Panels show snapshots of slip velocity distribution for one cycle, with the time between each snapshot indicated on top of the panels. The seismic slip (shown as red) only ruptures part of the velocity-weakening patch. The patch is indicated by a white box.

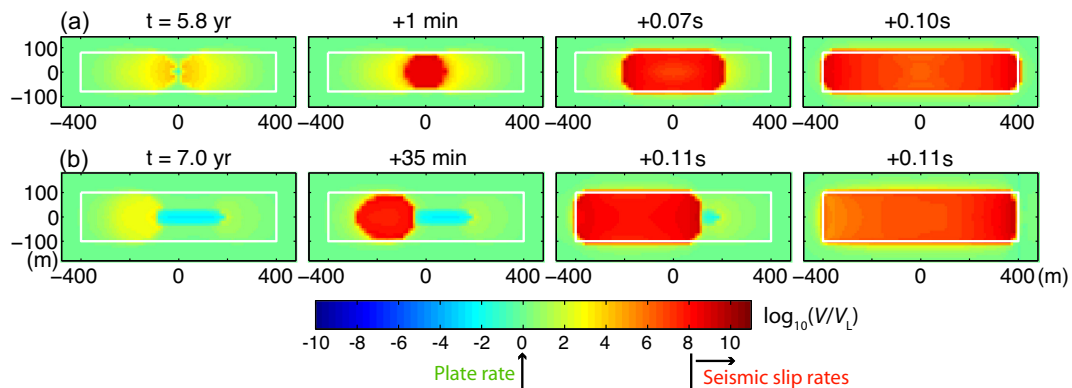


**Figure 6.** Example of an event of seismic pattern II with a rectangular patch. (a)  $r_{III}/h^* = 0.9$ ,  $r_{II}/h^* = 4.4$ . (b)  $r_{III}/h^* = 1.1$ ,  $r_{II}/h^* = 4.4$ . Snapshots of slip velocity distribution for one cycle with the time between each snapshot are shown. The seismic event ruptures the whole velocity-weakening patch.

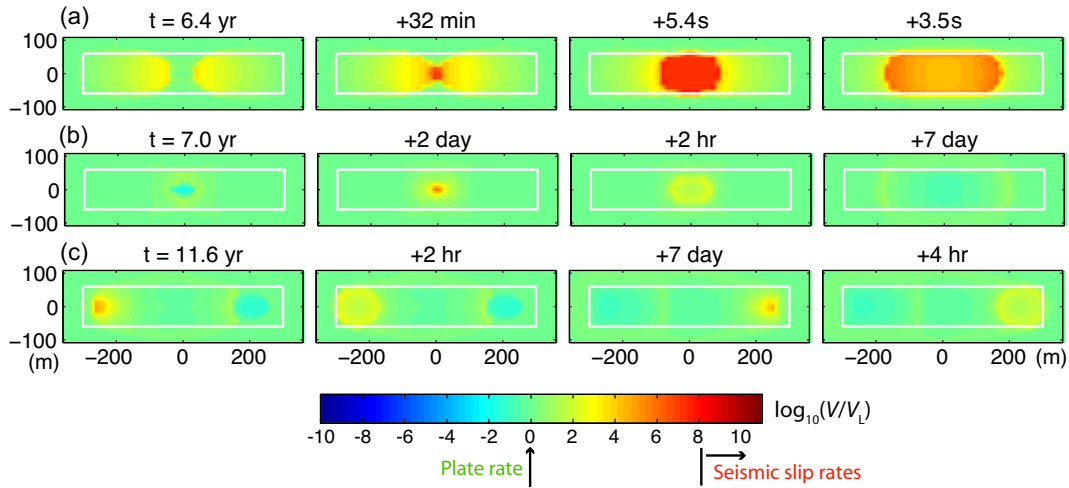


**Figure 7.** Example of non-characteristic event sequences with a rectangular patch ( $r_{III}/h^* = 0.7$ ,  $r_{II}/h^* = 3.3$ ): (a) a seismic event; (b) aseismic-slip event symmetric with respect to the centre of the patch; (c) aseismic-slip event that starts at one end.

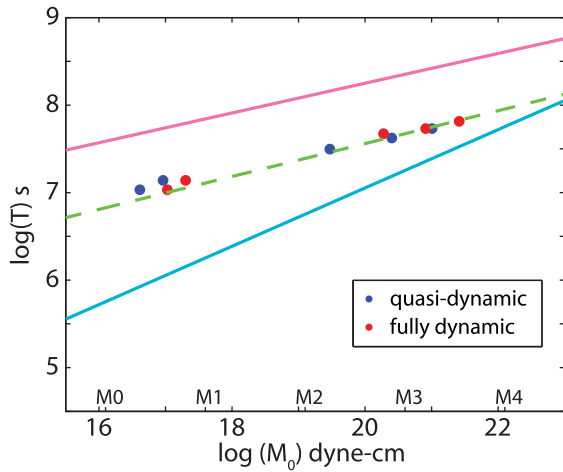


**Figure 8.** Recurrence time versus seismic moment for quasi-dynamic and fully dynamic simulations (aging form with  $a = 0.015$ ,  $b = 0.019$ ). The two approaches show similar scalings. The lines have the same meaning as in Fig. 2.

## 7 SIMULATED NUCLEATION PROCESSES

In this work, we have conducted simulations in both 2-D and 3-D models, and studied different forms of the state evolution law. Here we compare nucleation properties obtained in different simulations. Only fully dynamic simulations with a circular patch are considered.

One of the important characteristics of the earthquake initiation is the nucleation size, that is, the size of the zone slipping on the fault right before the seismic (wave-emitting) event. In our simulations, continuous slip in the velocity-strengthening region creates stress concentration inside the velocity-weakening patch, inducing aseismic slip there (e.g. Figs 5–7). This band of aseismic slip initiates at the boundaries of the patch and widens with time, spreading over the entire patch for sufficiently small patch radii  $r$ . As shown in Chen & Lapusta (2009), small enough patches remain completely aseismic. For each combination of model parameters, there is a critical patch size that starts producing seismic events (defined as slip with slip rate of  $0.1 \text{ m s}^{-1}$  or larger). It is natural to regard this critical patch size, which we denote by  $r_{\text{nuc}}$ , as a measure of the

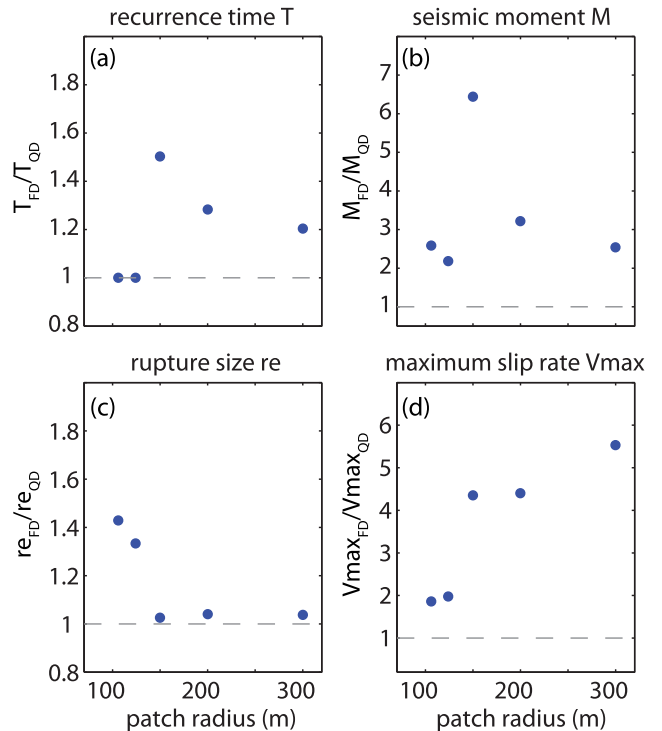


**Figure 9.** Ratios of results in fully dynamic (FD) simulations and quasi-dynamic (QD) simulations as functions of the patch radius, for (a) the recurrence time, (b) seismic moment, (c) effective rupture radius and (d) maximum slip rate.

nucleation half-size (the entire size being the diameter of the patch  $2r_{\text{nuc}}$ ). In the following, we show that  $r_{\text{nuc}}$  is indeed relevant for describing the nucleation behaviour of larger patches. The values of  $r_{\text{nuc}}$  in simulations with different forms of the state evolution law and different values of  $a$  and  $b$  are shown in Fig. 12. As expected based on prior studies (Rubin & Ampuero 2005; Ampuero & Rubin 2008), the aging form results in the largest values of  $r_{\text{nuc}}$ , followed by the slip and combined forms with similar  $r_{\text{nuc}}$ , and the composite form, which results in the smallest  $r_{\text{nuc}}$  among all 3-D simulations. Also as expected, the values of  $r_{\text{nuc}}$  are generally smaller for larger

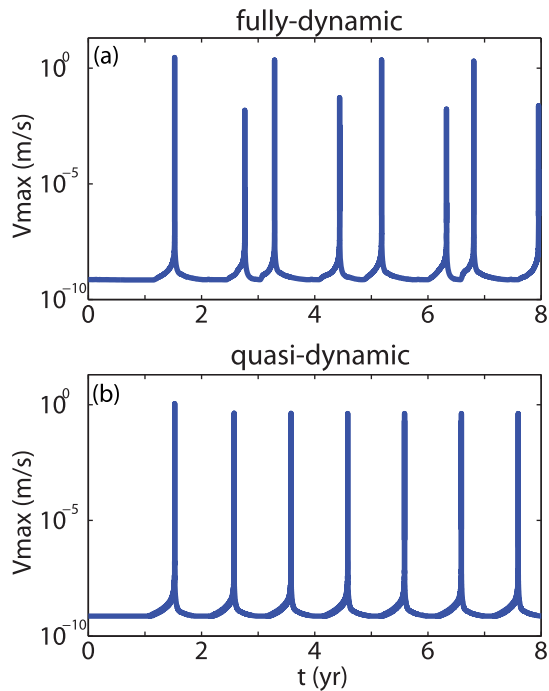


**Figure 10.** The maximum slip velocity on the fault as a function of time for (a) fully dynamic and (b) quasi-dynamic simulations. This example is for the aging form with  $a = 0.015$ ,  $b = 0.019$  and  $r = 150$  m. Quasi-dynamic simulations result in lower maximum slip velocity than fully dynamic simulations. The slip patterns can also be different for these two simulation approaches. In this example, the fully dynamic simulation has creep events between seismic events, but these creep events do not occur in the quasi-dynamic simulation. As a result, the recurrence time of seismic events in the fully dynamic simulation is almost twice larger.

values of  $(b - a)$  and  $r_{\text{nuc}}$  for 2-D simulations are smaller than those for 3-D simulations with the same state evolution law.

If  $r_{\text{nuc}}$  is indeed representative of the nucleation half-size in models with larger patches, then we would anticipate that, for patch radii  $1 \leq r/r_{\text{nuc}} \lesssim 2$ , the aseismic slip on the patch penetrates all the way to the centre of the patch before seismic events nucleate, while for  $r/r_{\text{nuc}} \gtrsim 2$ , the aseismic slip only penetrates a radial distance of  $2r_{\text{nuc}}$ , at which point a seismic event nucleates within this aseismically slipping band. This is exactly what we observe in our 3-D simulations. Fig. 13 illustrates two representative cases, with  $r/r_{\text{nuc}} = 1.2$  (left-hand column) and  $r/r_{\text{nuc}} = 11$  (right-hand column). In the case of  $r/r_{\text{nuc}} = 1.2 < 2$ , aseismic creep penetrates all the way to the centre of the patch, and the entire patch is slipping with slip rates above the loading rate when the seismic threshold is reached (Fig. 13, left-hand column). For simulations with the aging form and  $1 \leq r/r_{\text{nuc}} \lesssim 2$ , seismic ruptures usually also start from the centre of the patch (see Chen & Lapusta 2009 for examples). For simulations with the slip form and  $1 \leq r/r_{\text{nuc}} \lesssim 2$ , the nucleation zone keeps shrinking to one side and seismic ruptures usually start from the border of the patch (Fig. 13, left-hand column). When  $r/r_{\text{nuc}} = 11 > 2$ , aseismic creep only penetrates a certain radial distance into the patch, which is comparable to  $2r_{\text{nuc}}$ , and earthquakes nucleate in this penetrated region (Fig. 13, right-hand column). Let us denote this radial distance from the patch edge to creep front by  $r_{\text{creep}}$ . We compute  $r_{\text{creep}}$  as an average of the creep-penetrated radial distances in the horizontal and vertical directions (Fig. 1) when the maximum slip velocity reaches the seismic threshold of  $0.1 \text{ m s}^{-1}$ . Fig. 14 gives the values of  $r_{\text{creep}}/2r_{\text{nuc}}$  for different patch

sizes and a representative set of parameters  $a$  and  $b$ , for both 3-D and 2-D simulations with slip and aging forms of state evolution. As Fig. 14 shows,  $r_{\text{creep}}$  is indeed approximately constant for different patch sizes and approximately equal to  $2r_{\text{nuc}}$  for 3-D simulations. Note that the ratio  $r_{\text{creep}}/2r_{\text{nuc}}$  is a little larger for simulations with the slip form than for those with the aging form. Interestingly, 2-D simulations have larger  $r_{\text{creep}}/2r_{\text{nuc}}$  ratios, by about a factor of two, than 3-D simulations with the same state evolution law. The creep distance could be used to characterize the early phase of nucleation (Mitsui & Hirahara 2011).

For relatively small patch sizes, aseismic slip creeps all the way into the centre of the patch, and hence the seismic slip  $d_0$  at the centre of the patch is only a portion of the total slip  $V_L T$ . The ratio between the seismic slip and total slip at the centre of the patch is observed to increase with the patch size in our simulations, all the way to 1, as expected (Fig. 15a). When the patch size is large enough, aseismic slip only creeps into the patch for a distance of  $r_{\text{creep}}$ , thus the seismic slip at the centre of the patch is the same as the total slip. The transition of the ratio  $d_0/V_L T$  to 1 occurs when the patch radius is about equal to  $r_{\text{creep}}$ , or  $2r_{\text{nuc}}$  for 3-D simulations. The dependence of  $d_0/V_L T$  on the normalized patch radius is similar for 2-D and 3-D simulations with the aging and slip forms, with slight difference in the transition point, which is related to the difference in  $r_{\text{creep}}$ . The ratio between the seismic moment  $M_0$  and total moment on the patch  $\mu A V_L T$ , where  $A$  is the patch area, increases rapidly for patch radius smaller than  $r_{\text{creep}}$ , and more gradually for larger patch radius (Fig. 15b). A fraction of the total moment is released through aseismic slip even for relatively large patches, due to the aseismic slip in the creep-in zone around the patch boundary. Since  $M_0$  for seismic events is calculated as the seismic moment on the entire fault (the patch and the surrounding area), and seismic ruptures can penetrate into the velocity-strengthening area outside the patch, the ratio  $M_0/\mu A V_L T$  may be slightly larger than 1 for simulations with the larger patch radii. The dependence of the ratio  $d_0/V_L T$  or  $M_0/\mu A V_L T$  on the normalized patch size does not systematically depend on parameters  $a$  and  $b$  we studied, so Fig. 15 shows the results for one representative set of parameters  $a$  and  $b$ . The ratio  $d_0/V_L T$  is commonly defined as seismic coupling coefficient. Similar dependence of the coefficient on the size of velocity-weakening zone has been shown for different models (Kato & Hirasawa 1997).

Now that we have established that  $r_{\text{nuc}}$  is a relevant measure for estimating the extent of aseismic creep-in for larger patches, let us investigate which theoretical estimates match the simulated values of  $r_{\text{nuc}}$ . As introduced in Section 2, three different estimations (7–9) of nucleation half-size have been proposed. Fig. 16 shows the comparison between  $r_{\text{nuc}}$  and the proposed estimations of the nucleation half-length, for 2-D simulations with the aging and slip form. The results for the simulations with the aging form are in excellent agreement with  $h_{\text{RA}}^*$ . The results for the simulations with the slip form are better matched by  $h_{b-a}^*$  in terms of the dependence on parameters  $a$  and  $b$ ; the values of  $r_{\text{nuc}}$  are about two times larger than  $h_{b-a}^*$ . The fit of  $r_{\text{nuc}}$  by the estimations of the nucleation half-length for all the simulations is summarized in Table 1. For the sets of parameters  $a$  and  $b$  used in this study,  $r_{\text{nuc}}$  for the simulations with the aging form are best fitted by  $h_{\text{RA}}^*$ , and  $r_{\text{nuc}}$  for the simulations with the slip, combined and composite forms are best fitted by  $h_{b-a}^*$ . The fit of  $r_{\text{nuc}}$  by the corresponding best estimation of the nucleation half-length is better for 2-D simulations than 3-D simulations with the same state evolution laws. Note that the values in Table 1 do not depend on the constant prefactors of the nucleation size estimates.

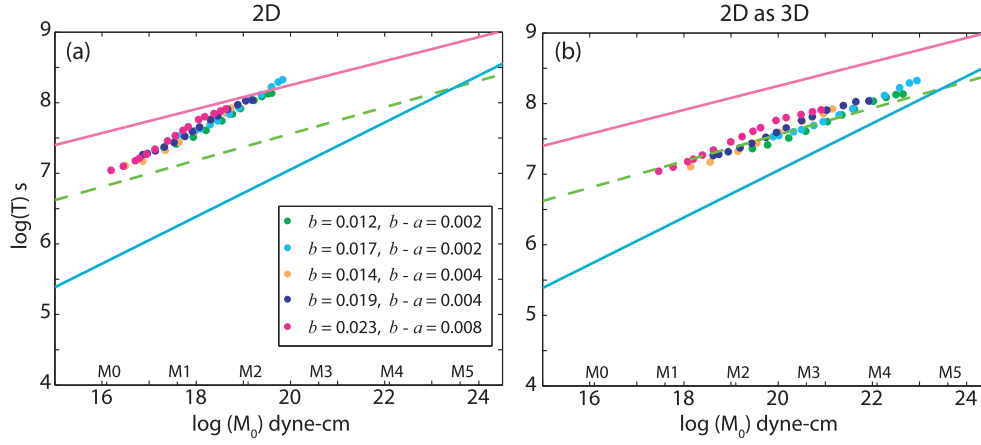


**Figure 11.** Simulations with a 2-D antiplane model (with the aging form). (a) If seismic moment is computed per unit length of the fault in 2-D, the scaling is quite different from that with the 3-D model and from the observed one. (b) When the results of 2-D simulations are interpreted in terms of a 3-D problem, the scaling is similar to that of the 3-D model. The lines have the same meaning as in Fig. 2.

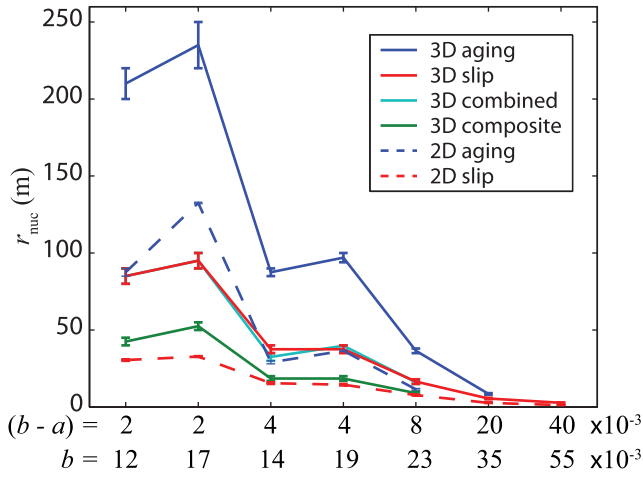


**Figure 12.** The smallest patch radius  $r_{\text{nuc}}$  that produces seismic events in the simulations with different sets of parameters  $a$ ,  $b$  and with different state evolution laws. Since the simulations are done with finite increments of patch radius,  $r_{\text{nuc}}$  is within the range indicated by the error bar, of which the lower end shows the largest simulated  $r$  that does not produce seismic events, and the upper end shows the smallest simulated  $r$  that does produce seismic events. Note that  $r_{\text{nuc}}$  is about the same for simulations with the slip form and combined form so that the corresponding lines are nearly on top of each other.

## 8 THEORETICAL MODEL FOR SCALING OF SEISMIC MOMENT WITH RECURRENCE TIME

As shown in Section 7, the simulated earthquakes can be divided into two regimes based on the ratio between the patch radius  $r$  and the nucleation half-length  $r_{\text{nuc}}$ . The numerically determined nucleation half-length  $r_{\text{nuc}}$  can be well approximated by the estimate  $h_{\text{RA}}^*$  for the aging form and  $h_{b-a}^*$  for the other forms, as discussed in Section 7, and these estimates are denoted by  $h^*$  here for simplicity. In 3-D simulations with a circular patch, for  $1 \lesssim r/h^* \lesssim 2$ , aseismic slip before seismic event penetrates all the way into the centre of the patch, and the entire patch slips aseismically before seismic event. For  $r/h^* \gtrsim 2$ , aseismic slip penetrates into the patch for the radial distance of only about  $2h^*$ , and the earthquake nucleates in this penetrated annular region.

Let us use the characteristic patch behaviour in these regimes to derive an approximate theoretical model for the scaling between the seismic moment and recurrence time. Note that the seismic event penetrates into the velocity-strengthening area, arresting there, and hence has the source dimension somewhat larger than the size of the velocity-weakening patch; the difference depends on the stress drop on the patch and the frictional properties of the surrounding velocity-strengthening region. However, for the frictional parameters used in this study, this effect is relatively small, and we ignore it for simplicity in our theoretical model, considering the radius of the patch-spanning seismic events to be  $r$ . We are also not considering the events with the size smaller than the velocity-weakening patch, which appear in some models, for example, the ones with the aging form of the state variable evolution (Chen & Lapusta 2009), but not others, for example, the ones with the slip form.

In the regime of  $1 \lesssim r/h^* \lesssim 2$  (Fig. 17), the stress levels before and after the earthquake,  $\tau_i$  and  $\tau_f$ , respectively, can be approximated as the steady-state stresses with slip velocities equal to loading velocity  $V_L$  ( $\sim 10^{-9}$  m s $^{-1}$ ) and dynamic slip velocity  $V_{\text{dyn}}$  ( $\sim 1$  m s $^{-1}$ ), respectively (Figs 17a,c). Let us denote the corresponding stress drop difference by  $\Delta\tau_{L-\text{dyn}}$ :

$$\begin{aligned} \Delta\tau_{L-\text{dyn}} &= \tau_i - \tau_f \approx \sigma [f_0 + (a - b) \ln(V_L/V_0)] \\ &\quad - \sigma [f_0 + (a - b) \ln(V_{\text{dyn}}/V_0)] \\ &= \sigma(b - a) \ln(V_{\text{dyn}}/V_L) \approx (9 \ln 10)(b - a)\sigma. \end{aligned} \quad (10)$$

The average static stress drop  $\Delta\tau$  for the seismic event is then close to this value,  $\Delta\tau = \Delta\tau_{L-\text{dyn}}$ . The seismic slip on the patch has the elliptical shape (Fig. 17b,d) expected from a circular crack model with a constant stress drop  $\Delta\tau$  (Eshelby 1957; Keilis-Borok 1959) and can indeed be well approximated by using the stress drop value equal to  $\Delta\tau_{L-\text{dyn}}$  (Fig. 17d, dashed line):

$$d(\rho) = \frac{24\Delta\tau}{7\pi\mu} \sqrt{r^2 - \rho^2} = \frac{24\Delta\tau_{L-\text{dyn}}}{7\pi\mu} \sqrt{r^2 - \rho^2}, \quad (11)$$

where  $\rho$  is the distance from the centre of the patch. We can also estimate the seismic moment as (Brune 1970):

$$M_0 = \frac{16}{7} \Delta\tau_{L-\text{dyn}} r^3. \quad (12)$$

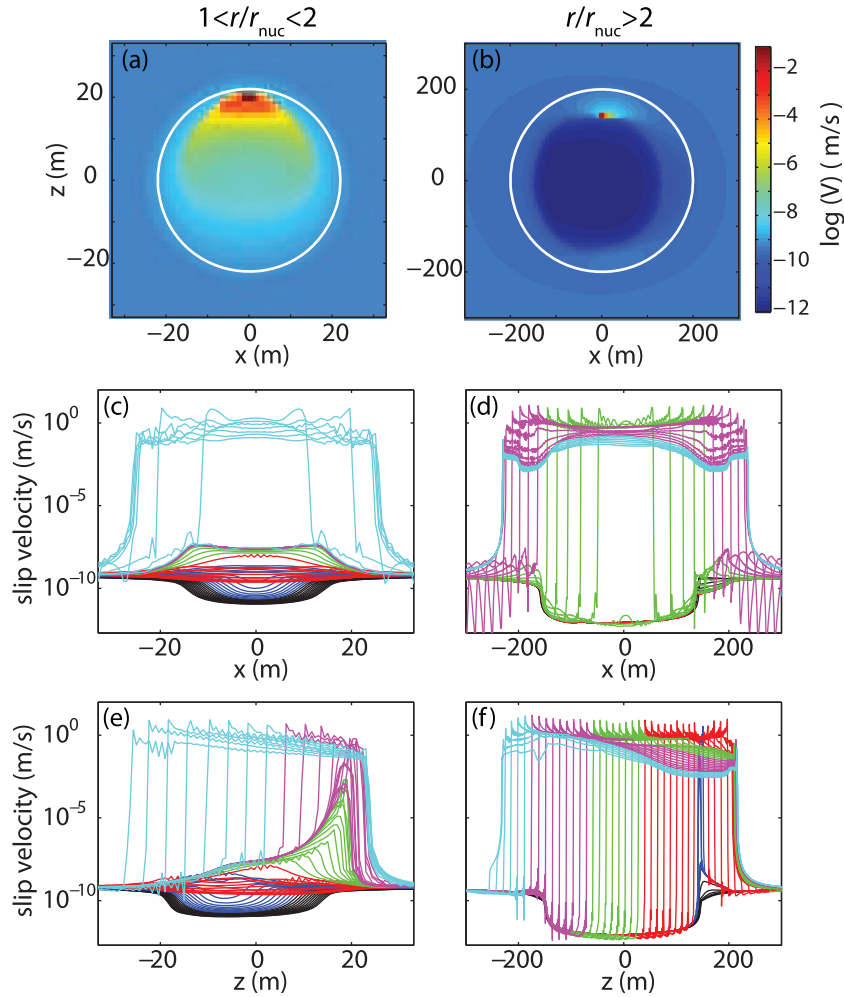


**Figure 13.** Representative nucleation processes for two  $r/r_{\text{nuc}}$  regimes:  $r/r_{\text{nuc}} = 1.2 < 2$  (left-hand column) and  $r/r_{\text{nuc}} = 11 > 2$  (right-hand column). The slip form of the state variable evolution is used. (a,b) Slip velocity distribution over part of the fault that includes the VW patch, when the maximum slip velocity reaches the seismic threshold of  $0.1 \text{ m s}^{-1}$ . (c–f) The nucleation and rupture processes in terms of the evolution of slip velocity along the  $x$ - (c–d) and  $z$ - (e–f) axes are plotted every several time steps (note that the time steps are variable). The time progression in the slip velocity profiles is illustrated through varied colours, with black, blue, red, green, magenta and cyan showing progressively later times.

If the centre of the patch slipped only seismically, we would expect that

$$T = d(0)/V_L = \frac{24\Delta\tau_{L-\text{dyn}}r}{7\pi\mu V_L}. \quad (13)$$

Based on eq. (11), this implies  $T \propto r \propto M_0^{1/3}$ . However, as shown in Fig. 15, the seismic slip is only part of the total slip on the centre of the patch for  $r/h^* \lesssim 2$ , and the ratio of seismic to total slip increases with  $r/h^*$ . Hence we expect a scaling between  $T$  and  $M_0$  with an exponent smaller than  $1/3$ , as the simulation results show.

In the regime of  $r/h^* \gtrsim 2$ , the recurrence time is determined by the time for the creep to penetrate the distance of  $2h^*$  into the patch so that the earthquake can nucleate. In that creeping portion of the patch, the stress evolves from  $\tau_f$  right after the previous seismic event to  $\tau_i$  before the next event, that is, increases by  $\Delta\tau_{L-\text{dyn}}$  (Figs 18a,c). The stressing rate at the location of  $2h^*$  inside the patch due to steady creep outside the patch can be expressed by (Das & Kostrov 1986):

$$\dot{\tau} = C \frac{\mu V_L}{\sqrt{r^2 - (r - 2h^*)^2}}, \quad (14)$$

where  $C$  is a model-dependent constant. Thus we can estimate the recurrence time  $T$  as

$$T = \frac{\Delta\tau_{L-\text{dyn}}}{C\mu V_L} \sqrt{r^2 - (r - 2h^*)^2}. \quad (15)$$

Our model differs from the model of Das & Kostrov (1986) in that the creep front changes, so we expect that the stressing rate is higher in our models and the expression (14) needs to be adjusted. An exact solution is not straightforward to obtain, since the speed of the creeping front is unknown and potentially variable. We approximately account for the difference by adjusting the constant  $C$  in Das & Kostrov (1986): for  $r = 2h^*$ , an intersection of the two regimes, we expect that the recurrence times calculated based on eqs (13) and (15) are the same, giving us  $C = 7\pi/24$ . Thus eq. (15) becomes:

$$T = \frac{24\Delta\tau_{L-\text{dyn}}}{7\pi\mu V_L} \sqrt{r^2 - (r - 2h^*)^2} = \frac{48\Delta\tau_{L-\text{dyn}}}{7\pi\mu V_L} \sqrt{rh^* - h^{*2}}. \quad (16)$$

The seismic slip on the annulus of thickness  $2h^*$  has an elliptical shape, and the seismic slip on the central circular patch area is approximately constant and nearly equal to  $V_L T$  because almost all the slip on the central area is accumulated seismically (Figs 18b,d).

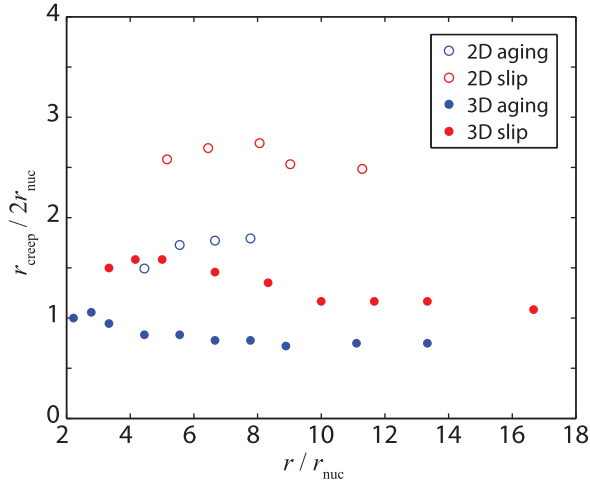


**Figure 14.** The ratio between the creep-in distance  $r_{\text{creep}}$  and the smallest patch dimension  $2r_{\text{nuc}}$  that produces seismic events.  $r_{\text{creep}}$  is about the same as  $2r_{\text{nuc}}$  for the simulated range of patch radii  $r$  in 3-D simulations with the aging or slip form, as expected. The ratio  $r_{\text{creep}}/2r_{\text{nuc}}$  is larger for simulations with the slip form than those with the aging form. 2-D simulations generally have larger  $r_{\text{creep}}/2r_{\text{nuc}}$  than 3-D simulations.

Thus we could estimate the seismic moment with the seismic slip distribution approximated by a truncated elliptical function. The approximation gives:

$$\begin{aligned} M_0 &= \frac{\mu\pi V_L T}{3} (2r^2 + (r - 2h^*)^2) \\ &= \frac{16\Delta\tau_{L-\text{dyn}}}{7} \sqrt{r h^* - h^{*2}} (3r^2 - 4r h^* + 4h^{*2}). \end{aligned} \quad (17)$$

The approximate theoretical scaling of  $T$  versus  $M_0$  based on eqs (16) and (17) (Fig. 19) is similar to our numerical results (Figs 3a,b), for both aging and slip forms and a range of friction properties. For  $r/(2h^*) \gg 1$ ,

$$T = \frac{48\Delta\tau_{L-\text{dyn}}}{7\pi\mu V_L} \sqrt{r h^*} \propto r^{1/2}, \quad (18)$$

and

$$M_0 = \frac{48\Delta\tau_{L-\text{dyn}}}{7} r^{5/2} \sqrt{h^*} \propto r^{5/2}. \quad (19)$$

Hence we have

$$T = \left(\frac{48}{7}\right)^{4/5} \frac{\Delta\tau_{L-\text{dyn}} h^{*2/5}}{\pi\mu V_L} M_0^{1/5} \propto M_0^{0.2}, \quad (20)$$

which is close to the observations of  $T \propto M_0^{0.17}$ . Note that this scaling is similar to the one derived in Cattania & Segall (2019) based on energy balance concepts, but has slightly different exponents; in both scalings, the loading rate  $V_L$  enters in the same way. The steeper scaling for smaller  $r/(2h^*)$  explains why some simulated results seem to deviate from the observed scaling if only a limited range of  $r/h^*$  is studied (Fig. 3).

Since  $h^*$  has different dependence on  $a$  and  $b$  for the aging form and slip form, as discussed in Section 7, we expect different dependence of  $T$  and  $M_0$  on  $a$  and  $b$  for the two forms. Let us consider the limit of  $r/(2h^*) \gg 1$ . For the aging form,  $h^* = (\pi^2/4)h_{\text{RA}}^*$ , and we get:

$$T = 15 \frac{(\sigma L b)^{2/5}}{V_L \mu^{3/5}} M_0^{1/5}, \quad (21)$$

For the slip form,  $h^* = 5h_{b-a}^*$  based on our simulations (Figs 14 and 16), and we get:

$$T = 20 \frac{[\sigma L(b-a)]^{2/5}}{V_L \mu^{3/5}} M_0^{1/5}, \quad (22)$$

Since the values of  $a$  and  $b$  used in our simulations result in larger variations in  $(b-a)$  than in  $b$ , we expect the simulated  $T$  with the slip form to show larger spread than that with the aging form, as Fig. 19 confirms. This difference is observed in the results of the numerical simulations as well (Fig. 3). The theoretically predicted dependence of  $T$  on  $L$  explains the simulation results from Chen & Lapusta (2009).

## 9 PARAMETER COMBINATIONS THAT ALLOW TO MATCH THE OBSERVED RANGES OF $T$ AND $M_0$

For the model parameters used in this study, the exponent of the simulated scaling between  $T$  and  $M_0$  is similar to the observation. However, the simulated absolute value of  $T$  for a given  $M_0$  is about five times smaller than the observation (Fig. 3). One way to match the observed absolute values of  $T$  is to decrease  $V_L$  from 23 to 4.5 mm a<sup>-1</sup> as done in Chen & Lapusta (2009); it is consistent with the theoretical scaling (20). Based on eq. (20), other solutions may also exist, and here we explore the possibilities.

As we vary parameters in eq. (20) to match the values of  $T$ , the seismic moment of the smallest seismic event that can be produced in this model, which we denote  $M_{0s}$ , may also change. For example, as explored in Chen & Lapusta (2009) and supported by eq. (20), larger values of  $L$  increase the recurrence times but they also increase the nucleation size and hence the size of the smallest seismic events that can be produced. For the smallest events that rupture the entire patch,  $r = h^*$  and the seismic moment of the smallest event, from eq. (17), can be expressed as:

$$M_{0s} = \frac{16}{7} \Delta\tau_{L-\text{dyn}} h^{*3}. \quad (23)$$

Then the moment magnitude of the smallest events is given by:

$$M_s = (\log M_{0s} - 9.1)/1.5. \quad (24)$$

For the standard logarithmic rate and state formulations considered in this study, eq. (23) can be written as:

$$M_{0s} = 23 \frac{(\mu L b)^3}{\sigma^2 (b-a)^5} \quad (\text{the aging form}) \quad (25)$$

or

$$M_{0s} = 191 \frac{(\mu L)^3}{\sigma^2 (b-a)^2} \quad (\text{the slip form}). \quad (26)$$

$M_s$  should be consistent with moment magnitudes as small as 0 to 1 (Nadeau & Johnson 1998). For example, increasing only  $L$  to match  $T$  would not be an acceptable solution, since  $M_{0s}$  is rapidly increasing with  $L$ . Smaller events may result from partial ruptures of the seismogenic patch, but such events result only in some models, notably with the aging form of the state variable evolution, but not in others. If we could produce partial ruptures of patches with the size of  $r = h^*$  for a wider range of conditions, for example, by including other mechanisms such as dilatancy, the constraint on the smallest magnitude of the events can be relaxed.

Based on the developed theoretical model for scaling (eqs 21 and 22) and the smallest moment expression (eqs 25 and 26), one way to match observations is to decrease  $\mu$ . Indeed, such approach was

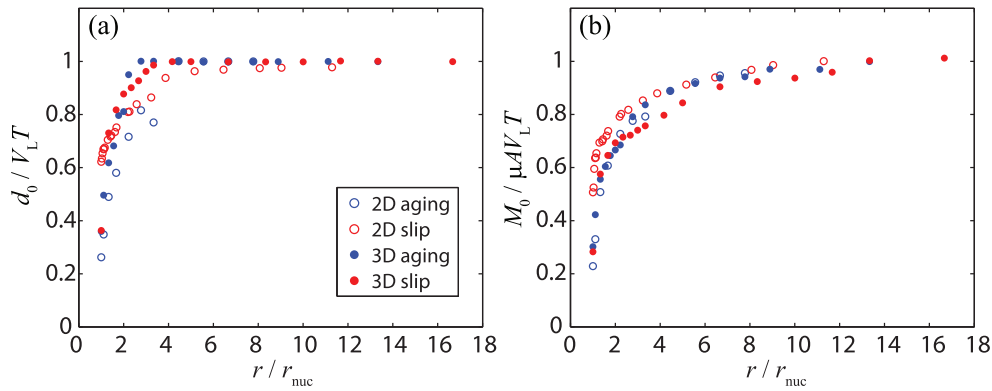


**Figure 15.** (a) The ratio between the seismic slip  $d_0$  at the centre of the patch and the total slip  $V_L T$  in one earthquake cycle, plotted versus the patch radius. (b) The ratio between the seismic moment  $M_0$  and the total moment  $\mu A V_L T$  of one earthquake cycle on the patch versus the patch radius.

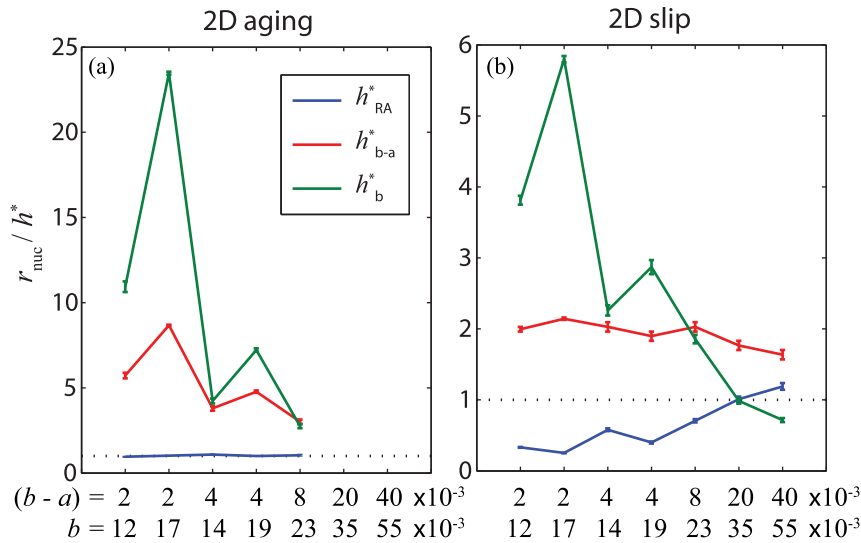


**Figure 16.** The ratio between the simulated nucleation half-size  $r_{\text{nuc}}$  and theoretical estimates of the nucleation half-size  $h^*$  for different sets of parameters  $a, b$ . Three different estimations of  $h^*$  are used, as discussed in the text. The dotted line illustrates how the perfect fit would look. (a) The simulated values of  $r_{\text{nuc}}$  for a 2-D antiplane model with the aging form are better fitted by  $h_{\text{RA}}^*$ . (b) The simulated values of  $r_{\text{nuc}}$  for a 2-D antiplane model with the slip form are better fitted by  $h_{b-a}^*$ , with the difference by a factor of about 2.

**Table 1.** Standard deviation of normalized  $r_{\text{nuc}}/h^*$  for different estimations of nucleation half-length  $h^*$  and simulations with different state evolution forms<sup>a</sup>

	$\text{std} \left[ \frac{r_{\text{nuc}}/h_{\text{RA}}^*}{\text{mean}(r_{\text{nuc}}/h_{\text{RA}}^*)} \right]$	$\text{std} \left[ \frac{r_{\text{nuc}}/h_{b-a}^*}{\text{mean}(r_{\text{nuc}}/h_{b-a}^*)} \right]$	$\text{std} \left[ \frac{r_{\text{nuc}}/h_b^*}{\text{mean}(r_{\text{nuc}}/h_b^*)} \right]$
2-D aging	<b>0.05</b>	0.42	0.85
2-D slip	0.55	<b>0.09</b>	0.67
3-D aging	<b>0.22</b>	0.31	0.74
3-D slip	0.46	<b>0.21</b>	0.79
3-D combined	0.25	<b>0.17</b>	0.60
3-D composite	0.30	<b>0.17</b>	0.62

<sup>a</sup> The smallest standard deviation for each model (a combination of 2-D/3-D and a state evolution form) is highlighted in bold.

suggested in previous studies (e.g. Dreger *et al.* 2007). However,  $\mu$  would need to be decreased to about 2 GPa. Such low shear modulus, however, is not clearly supported by observations, even for damage zones (Jeppson *et al.* 2010). Hence, in the following, we set  $\mu = 30$  GPa and consider the combined variations of other parameters for models with the slip form of the state variable evolution; models with the aging form can be analysed similarly.

For slip form of the state variable evolution, the theoretical scaling is described by eq. (22). We define  $H = T/M_0^{1/5}$  to represent the proportional scaling between predicted  $T$  and  $M_0$ , and compare it with the observation ( $H_{\text{obs}}$ ).  $H_{\text{obs}} = 5e5$  is determined for an average value of  $M_0$  representing the data. Based on the observations from Nadeau & Johnson (1998), this value of  $M_0$  corresponds to an approximate magnitude of 1.

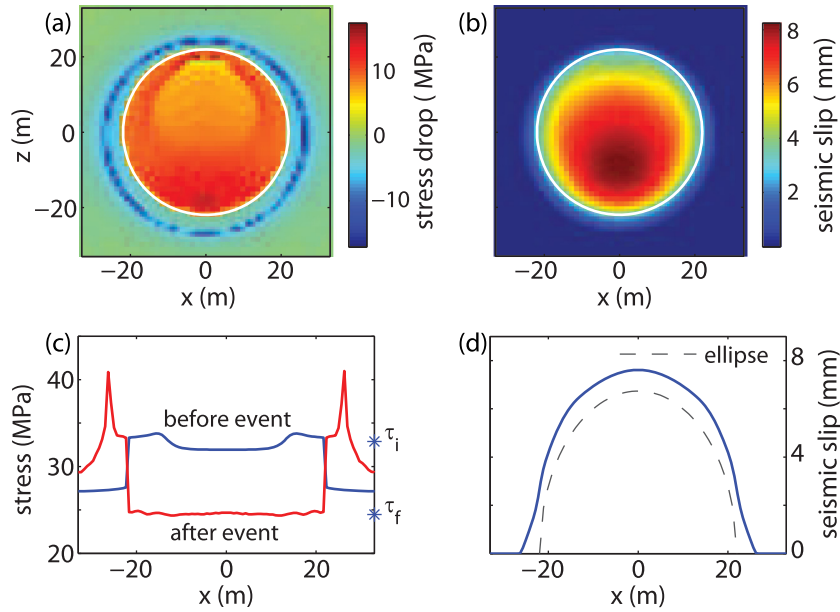


**Figure 17.** Example of stress drop and seismic slip for events with  $1 \lesssim r/h^* \lesssim 2$  (with the slip form,  $a = 0.015$ ,  $b = 0.023$ ,  $r/h^* \approx 1.2$ ): (a,b) maps of stress drop and seismic slip over the fault, (c,d) values for the cross-section along the  $x$  direction and through the centre of the patch. Estimated stress levels before ( $\tau_i$ ) and after ( $\tau_f$ ) the earthquake from eq. (10) are indicated as asterisks. Stress drop is approximately constant in this case, and the seismic slip has a shape similar to the elliptical function from eq. (11) (dashed line in d).

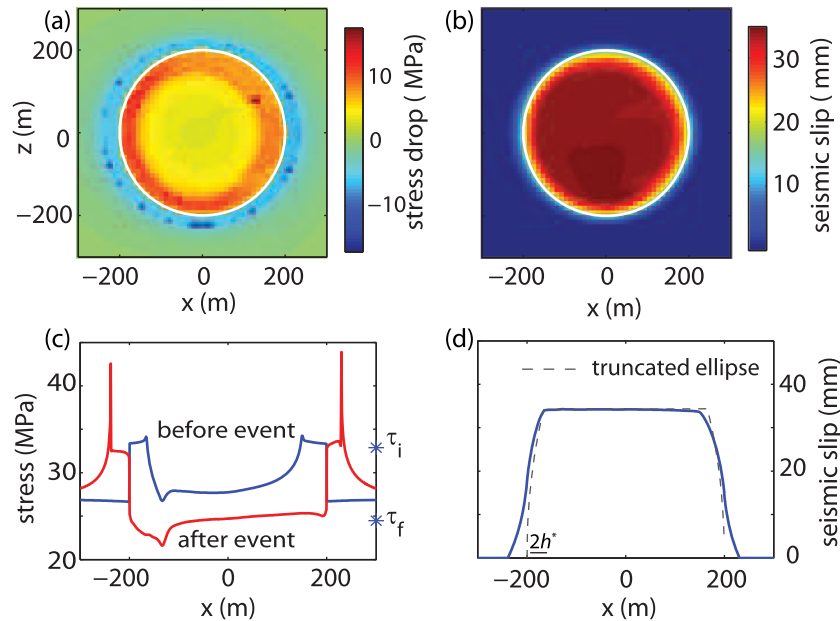


**Figure 18.** Example of stress drop and seismic slip for events with  $r/h^* \gtrsim 2$  ( $r/h^* \approx 11$  for the case shown). Plotting conventions are the same as in Fig. 17. Stress drop is smaller in the centre of the patch, and the seismic slip can be approximated with a truncated elliptical function.

First, let us consider the combinations of parameters  $L$  and  $\sigma(b-a)$  that would allow the model to match observations for  $V_L = 23 \text{ mm a}^{-1}$ . As shown in Fig. 20, the values of  $\sigma(b-a)$  that would match the observed recurrence times and the smallest events of  $M_w$  1.0 (or smaller) are larger than about 8 MPa. If  $(b-a) \approx 0.01 - 0.02$ , an upper bound of the values observed in the lab, this value of  $\sigma(b-a)$  requires  $\sigma \gtrsim 400 - 800$  MPa, which is only realistic if large local variations in compressive stress exist, for example, due to fault non-planarity (Sagy *et al.* 2007; Dunham *et al.* 2011). In that case, repeating earthquakes occur on highly compressed patches which

may also explain why the patches are velocity-weakening. If  $\sigma = 100$  MPa, then  $(b-a) \gtrsim 0.08$ , about an order of magnitude larger than what is observed in the lab, and perhaps suggestive of enhanced dynamic weakening. Such scenarios for repeating earthquakes have been considered in simulations presented in Lui & Lapusta (2018) and indeed shown to reproduce the observed scaling of the seismic moment with the recurrence time. Moreover, such scenarios also reproduce the relatively high stress drops inferred for the SF repeaters at Parkfield, with the average stress drop of 25 MPa or more

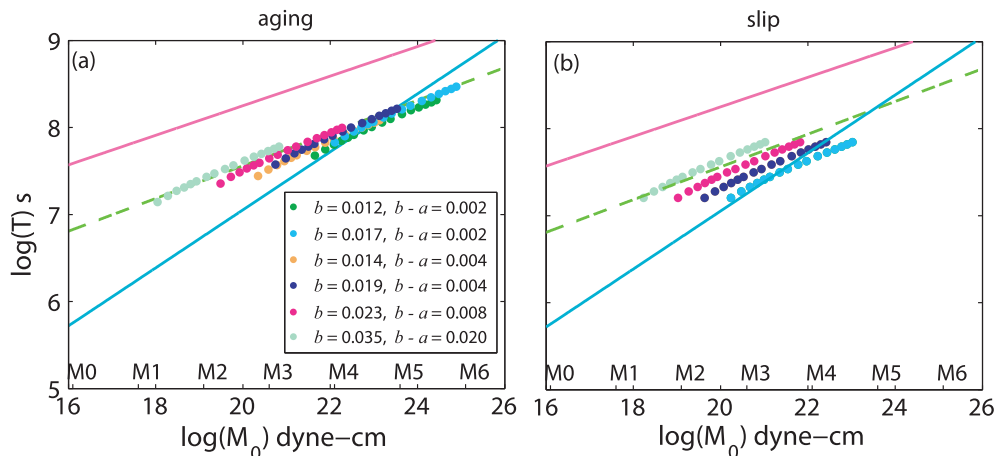


**Figure 19.** Seismic moment and recurrence time for 3-D fault models with the (a) aging form and (b) slip form estimated based on the theoretical approximations (10), (16) and (17). For each set of  $a$  and  $b$ , patch radius  $r$  is varied so that  $r/h^*$  ranges from 2 to 20.  $h^* = (\pi^2/4)h_{RA}^*$  for the aging form and  $h^* = 5h_{b-a}^*$  for the slip form based on our numerical simulations. The theoretically estimated scaling is similar to the numerically simulated scaling (green dashed line). The lines have the same meaning as in Fig. 2.

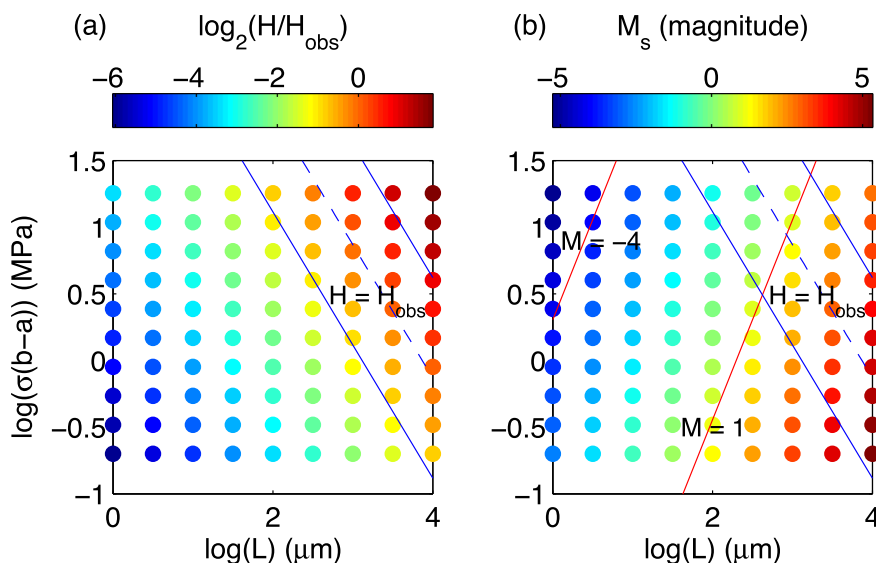


**Figure 20.** Effect of variations in  $\sigma(b-a)$  and  $L$  on the recurrence time and smallest seismic moment for the slip form based on eqs (22) and (26);  $\mu = 30$  GPa and  $V_L = 23$  mm  $a^{-1}$  are used. (a) Values of  $T$  from eq. (22), plotted as  $H = T/M_0^{1/5}$ , normalized by the value that matches the observations ( $H_{obs}$ ). The contour of  $H = H_{obs}$  is indicated by the dashed line, with the parallel solid lines indicating  $H = 2H_{obs}$  and  $H = 0.5H_{obs}$ . (b) The moment magnitude of the smallest events that can be produced based on eq. (26). Contours of  $M = -4$  and  $M = 1$  are plotted. The values of  $\sigma(b-a)$  and  $L$  that allow us to both have long enough recurrence times and the smallest events of  $M_w$  1.0 or smaller are larger than about 8 MPa and smaller than  $1e3$   $\mu$ m, respectively.

and local stress drops as high as 60–90 MPa (Dreger *et al.* 2007; Abercrombie 2014).

Now, let us consider smaller values of  $\sigma(b-a)$  and determine how much smaller than  $23$  mm  $a^{-1}$   $V_L$  needs to be for the standard logarithmic rate- and state-model to reproduce the observed values of  $T$ . If  $\sigma(b-a) = 0.2$  MPa, a typical value in this study and Chen & Lapusta (2009), then  $V_L$  needs to be as small as  $2$  mm  $a^{-1}$  (Fig. 21). Note that this is for the slip form; simulations with the aging form reproduce observations for a higher value of  $V_L = 4.5$  mm  $a^{-1}$ . If  $\sigma(b-a) = 2$  MPa, based on  $\sigma = 100$  MPa and  $(b-a) = 0.02$ , on the high side of potential rate-and-state values, then  $V_L$  can be up to about  $9$  mm  $a^{-1}$  (Fig. 22), potentially reasonable for the transitional region between creeping and locked segments where most of the repeating earthquakes are observed at Parkfield (e.g. Barbot *et al.* 2012). So with the standard logarithmic rate and state friction laws

and no enhanced local compression,  $V_L$  needs to be much smaller than  $23$  mm  $a^{-1}$  to match observations.

## 10 DISCUSSION

In the model for the repeating sequences based on standard rate-and-state friction as considered in this study, the stress drop has some variation with the event size, for a given set of friction properties; however, this variation would likely not be possible to observe in natural earthquake sequences. The stress drop is approximately constant for  $1 \lesssim r/h^* \lesssim 2$ . For  $r/h^* \gtrsim 2$ , the nucleation happens as soon as the annulus of  $2h^*$  reaches the stress level of  $\Delta\tau$ . One consequence is that, for the larger patch sizes, the centre of the patch is less stressed, and thus the average stress drop over the patch decreases. The behaviour of stress drops in these two regimes is

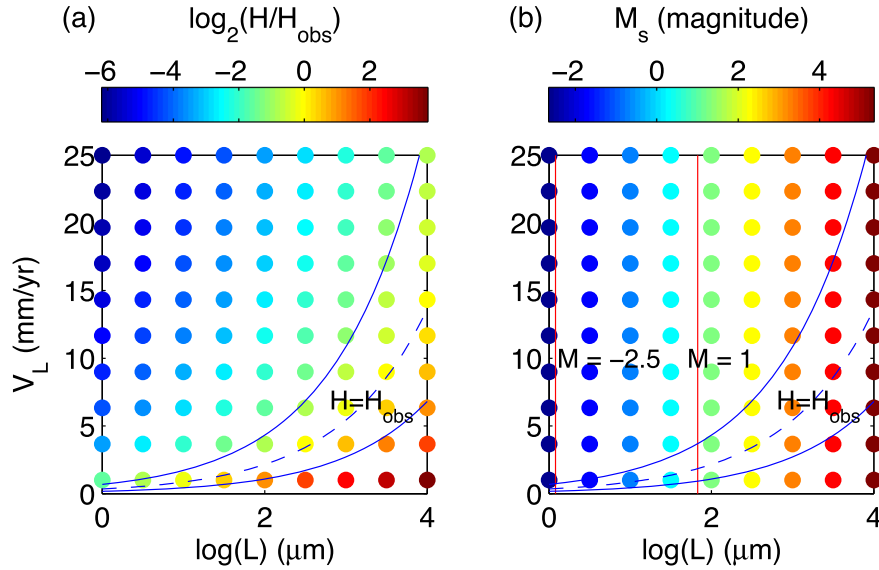


**Figure 21.** Effect of variations in  $V_L$  and  $L$  on the recurrence time and smallest seismic moment for the slip form based on eqs (22) and (26);  $\mu = 30$  GPa and  $\sigma(b - a) = 0.2$  MPa are used. (a) Values of  $T$  from eq. (22), plotted as  $H = T/M_0^{1/5}$ , normalized by the value that matches the observation ( $H_{\text{obs}}$ ). The contour of  $H = H_{\text{obs}}$  is indicated by the dashed line, with the parallel solid lines indicating  $H = 2H_{\text{obs}}$  and  $H = 0.5H_{\text{obs}}$ . (b) The moment magnitude of the smallest events that can be produced based on eq. (26). Contours of  $M = -2.5$  and  $M = 1$  are plotted.

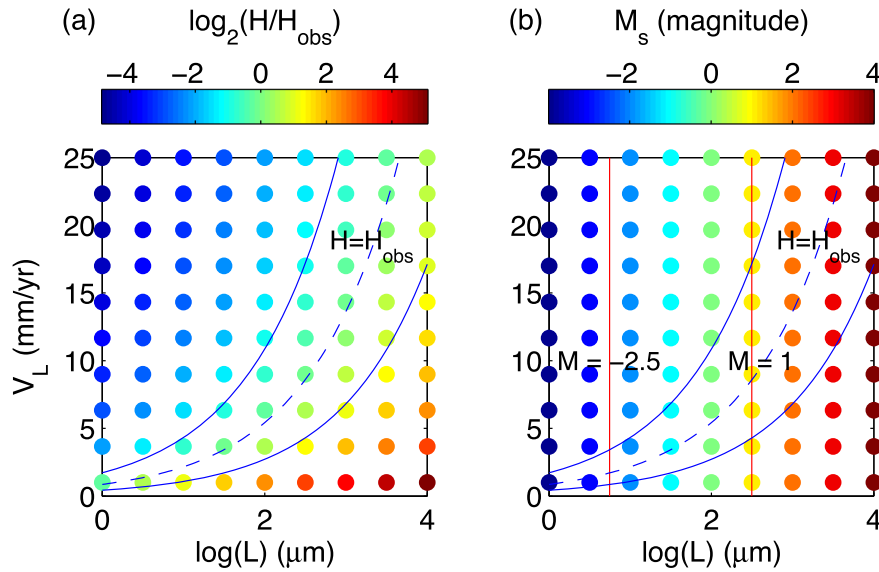


**Figure 22.** Similar to Fig. 21 but with  $\sigma(b - a) = 2$  MPa.

consistent with the findings of Kato (2012), where a slightly different problem is considered. While our theoretical consideration predicts that the average stress drop would continue to get smaller for larger  $r/h^*$ , the model is likely invalid for  $r/h^*$  so large that the shear stress close to the middle of the patch becomes too low for the rupture to propagate; then, smaller events at the boundary of the patch would start to occur and the repeating nature of the produced seismic events would likely disappear (Wu & Chen 2014). This implies that the observed repeating sequences have the values of  $r/h^*$  within a certain range. For example, in our simulations with the slip form and  $b - a = 0.02$ , we have periodic behaviour for  $r/h^*$  from 1 to 17. The corresponding seismic moments span a range of about two magnitudes, while the area-averaged stress drops only differ by a factor smaller than 2. Such small variations in stress drop would not be easy to determine observationally, especially given the likely

variation in friction properties of the earthquake-producing patches and hence the corresponding scatter in stress drop values. Note that since  $h^*$  depends on a number of parameters such as  $a$ ,  $b$ ,  $L$  and  $\sigma$ , larger  $r/h^*$  does not necessarily imply larger  $r$  and larger magnitude of events. One would then expect a scatter of stress drops with magnitudes due to the variations of  $a$ ,  $b$ ,  $L$  and/or  $\sigma$ .

We find a slightly different scaling of the average seismic slip on the patch than that in Kato (2012). Based on our theoretical approximation, for  $r/(2h^*) \gg 1$ , the average seismic slip  $d$  on the patch can be expressed as:

$$d \propto V_L T \propto (f_i - f_f) \sqrt{\frac{\sigma L r}{\mu}}, \quad (27)$$

where  $f_i$  and  $f_f$  are the effective friction coefficients before and after the earthquake, that is,  $f_i = \tau_i/\sigma$  and  $f_f = \tau_f/\sigma$ . The square root

dependence of  $d$  on  $\sigma Lr/\mu$  agrees with the study that considers the balance between the fracture energy and energy release rate in a similar model (Kato 2012). The consideration in Kato (2012) leads to slightly different dependence of  $d$  on the frictional coefficients, with

$$d \propto \sqrt{f_p - f_f} \sqrt{\frac{\sigma Lr}{\mu}}, \quad (28)$$

where  $f_p$  is the peak (yield) friction coefficient. To differentiate between these two models, we have conducted two simulations with the same parameters except that one has enhanced dynamic weakening and hence lower  $f_f$ . We use the thermal pore pressurization mechanism to achieve enhanced dynamic weakening while keeping the slip weakening distance about the same, following Noda & Lapusta (2010). We find that, comparing the results with the standard logarithmic rate and state formulations, for the case with enhanced dynamic weakening, the effective  $(f_i - f_f)$  is about three times larger,  $\sqrt{f_p - f_f}$  is about 1.3 times larger, and the average seismic slip is about three times larger. Thus the model based on the nucleation time consideration (eq. 27) quantitatively explains the results better than the model based on the balance between the fracture energy and energy release rate (eq. 28). Note that the main focus of Kato (2012) is not on the dependence of  $d$  on the frictional coefficients, but on the scaling between  $d$  and  $\sigma D_c$ , where  $D_c$  is the slip weakening distance and proportional to  $L$ . So the main discussion in Kato (2012) is not affected by this difference.

The theoretical consideration we propose is useful for understanding some observations and numerical simulation results. Considering repeating earthquake sequences on different faults, it is reasonable to assume that they have similar values of shear modulus  $\mu$ , typical values of stress drops, and a similar range of the ratio between the patch sizes and nucleation sizes. Eq. (20) then predicts that the scaling between the recurrence time and seismic moment for repeating earthquake sequences on different faults should differ mostly due to differences in loading velocity  $V_L$ . This is exactly what observations show (Chen *et al.* 2007). The fact that the scaling between  $T$  and  $M_0$  for quasi-dynamic simulations is similar to the fully dynamic simulations also makes sense, because, for the patch sizes larger than the nucleation size, the recurrence time is determined by the nucleation time, which is a quasi-static process.

The theoretical model we propose only considers the seismic events that rupture the whole velocity-weakening patch. The seismic events that rupture only a part of the patch are observed with the aging form, especially for smaller  $(b - a)$ . The two types of events together also follow the observed  $T \propto M_0^{0.17}$  scaling (Figs 3a and 4a). An explanation for such behaviour has been proposed by Catania & Segall (2019).

The loading velocity of  $23 \text{ mm a}^{-1}$  is used in this study following Nadeau & Johnson (1998), to make direct comparison with the study of Chen & Lapusta (2009). As shown in Chen & Lapusta (2009), decreases in  $V_L$  as large as five times do not change the exponent of the scaling between  $T$  and  $M_0$  or the smallest magnitude of the events that can be produced, but only move the absolute values of  $T$  up and down. Note that an orders-of-magnitude change in  $V_L$ , as could occur during post-seismic slip due to a nearby large earthquake, may significantly change the seismic moment (Chen *et al.* 2010) and hence the scaling.

## 11 CONCLUSIONS

We have investigated the behaviour of small repeating earthquakes under different scenarios, including different state evolution forms, rectangular versus circular patch, quasi-dynamic versus fully dynamic simulations and 2-D versus 3-D simulations. We find that, with proper interpretation, the overall scaling of the recurrence time and seismic moment is similar in all these models. Differences in other characteristics of the repeating sequences do exist. For example, we find that the simulated nucleation half-length for simulations with the aging form is better approximated by  $h_{RA}^*$ , while that with the slip form is better approximated by  $h_{b-a}^*$ , consistent with differences between models with the two forms found in previous studies (Ampuero & Rubin 2008). This different dependence of the nucleation half-length on parameters  $a$  and  $b$  results in (relatively minor) differences in scaling of  $T$  and  $M_0$  for simulations with the aging and slip form.

We propose a simplified theoretical consideration for the simulated scaling that captures the occurrence of the aseismic slip on the patch and explains why the simulated scaling matches the observations. One of the main ingredients is that, for patch radii larger than the full nucleation size, the recurrence time is determined by the time for the creep to penetrate the distance of the full nucleation size into the patch. The obtained theoretical insight has been used to find the combinations of fault properties that allow the model to fit the observed scaling and range of the seismic moment and recurrence time. For the standard logarithmic rate and state friction laws and typically considered values of  $\sigma(b - a)$  (such as 0.2 to 2 MPa),  $V_L$  needs to be several times smaller than  $23 \text{ mm a}^{-1}$  to match the observations. If  $V_L$  is indeed close to  $23 \text{ mm a}^{-1}$  in the area of repeating earthquakes, then the required  $\sigma(b - a)$  needs to be larger than 8 MPa, pointing to either much larger local compression or enhanced dynamic weakening at the locations of the repeating sequences, as investigated in the numerical modelling of Lui & Lapusta (2018).

## ACKNOWLEDGEMENTS

This study was supported by the National Science Foundation (grants EAR-1520907, 1724686) and United States Geological Survey (grants G10AP00031 and G16AP00117). The numerical simulations for this research were performed on Caltech Division of Geological and Planetary Sciences Dell cluster. We thank Yi Liu and Hiroyuki Noda for the help with the code used to perform the simulations, Pablo Ampuero for helpful suggestions and two anonymous reviewers for their insightful and constructive comments.

## REFERENCES

- Abercrombie, R.E., 2014. Stress drops of repeating earthquakes on the San Andreas fault at Parkfield, *Geophys. Res. Lett.*, **41**(24), 8784–8791.
- Ampuero, J.-P. & Rubin, A.M., 2008. Earthquake nucleation on rate and state faults - aging and slip laws, *J. geophys. Res.*, **113**, B01302, doi:10.1029/2007JB005082.
- Barbot, S., Lapusta, N. & Avouac, J.-P., 2012. Under the hood of the earthquake machine: toward predictive modeling of the seismic cycle, *Science*, **336**(6082), 707–710.
- Beeler, N.M., Lockner, D.L. & Hickman, S.H., 2001. A simple stick-slip and creep-slip model for repeating earthquakes and its implication for microearthquakes at Parkfield, *Bull. seism. Soc. Am.*, **91**(6), 1797–1804.
- Ben-Zion, Y. & Rice, J.R., 1995. Slip patterns and earthquake populations along different classes of faults in elastic solids, *J. geophys. Res.*, **100**(B7), 12 959–12 983.

- Bhattacharya, P., Rubin, A.M., Bayart, E., Savage, H.M. & Marone, C., 2015. Critical evaluation of state evolution laws in rate and state friction: fitting large velocity steps in simulated fault gouge with time-, slip-, and stress-dependent constitutive laws, *J. geophys. Res.*, **120**(9), 6365–6385.
- Bhattacharya, P., Rubin, A.M. & Beeler, N.M., 2017. Does fault strengthening in laboratory rock friction experiments really depend primarily upon time and not slip? *J. geophys. Res.*, **122**(8), 6389–6430.
- Brune, J.N., 1970. Tectonic stress and the spectra of seismic shear waves from earthquakes, *J. geophys. Res.*, **75**(26), 4997–5009.
- Cattania, C. & Segall, P., 2019. Crack models of repeating earthquakes predict observed moment-recurrence scaling, *J. geophys. Res.*, **124**(1), 476–503.
- Chen, K.H., Nadeau, R.M. & Rau, R.-J., 2007. Towards a universal rule on the recurrence interval scaling of repeating earthquakes? *Geophys. Res. Lett.*, **34**, L16308, doi:10.1029/2007GL030554.
- Chen, K.H., Bürgmann, R., Nadeau, R.M., Chen, T. & Lapusta, N., 2010. Postseismic variations in seismic moment and recurrence interval of repeating earthquakes, *Earth planet. Sci. Lett.*, **299**(1-2), 118–125.
- Chen, T. & Lapusta, N., 2009. Scaling of small repeating earthquakes explained by interaction of seismic and aseismic slip in a rate and state fault model, *J. geophys. Res.*, **114**, B01311.
- Das, S. & Kostrov, B.V., 1986. Fracture of a single asperity on a finite fault: a model for weak earthquakes?, in *Earthquake Source Mechanics*, pp. 91–96, eds. Das, S., Boatwright, J. & Scholz, C.H., American Geophysical Union, Washington.
- Dieterich, J.H., 1979. Modeling of rock friction 1. Experimental results and constitutive equations, *J. geophys. Res.*, **84**(B5), 2161–2168.
- Dieterich, J.H., 1981. Constitutive properties of faults with simulated gouge, in *Mechanical Behavior of Crustal Rocks, vol.24 of Geophys. Monogr. Ser.*, pp. 103–120, eds. Handin, J. & Carter, N.L., AGU, Washington, D. C.
- Dieterich, J.H., 1992. Earthquake nucleation on faults with rate- and state-dependent strength, *Tectonophysics*, **211**(1-4), 115–134.
- Dieterich, J.H., 2007. Applications of rate- and state-dependent friction to models of fault slip and earthquake occurrence, in *Treatise on Geophysics, vol.4*, pp. 107–129, ed. Kanamori, H., Elsevier, Amsterdam.
- Dreger, D., Nadeau, R.M. & Chung, A., 2007. Repeating earthquake finite source models: Strong asperities revealed on the San Andreas fault, *Geophys. Res. Lett.*, **34**, L23302, doi:10.1029/2007GL031353.
- Dunham, E.M., Belanger, D., Cong, L. & Kozdon, J.E., 2011. Earthquake ruptures with strongly rate-weakening friction and off-fault plasticity, part 2: Nonplanar faults, *Bull. seism. Soc. Am.*, **101**, 2308–2322.
- Eshelby, J.D., 1957. The determination of the elastic field of an ellipsoidal inclusion, and related problems, *Proc. R. Soc. Lond. A.*, **241**(1226), 376, doi:10.1098/rspa.1957.0133.
- Hillers, G., Ben-Zion, Y. & Mai, P.M., 2006. Seismicity on a fault controlled by rate- and state-dependent friction with spatial variations of the critical slip distance, *J. geophys. Res.*, **111**, B01403, doi:10.1029/2005JB003859.
- Hirose, H. & Hirahara, K., 2002. A model for complex slip behavior on a large asperity at subduction zones, *Geophys. Res. Lett.*, **29**(22), 2068.
- Hori, T., Kato, N., Hirahara, K., Baba, T. & Kaneda, Y., 2004. A numerical simulation of earthquake cycles along the Nankai Trough in southwest Japan: lateral variation in frictional property due to the slab geometry controls the nucleation position, *Earth planet. Sci. Lett.*, **228**, 215–226.
- Igarashi, T., Matsuzawa, T. & Hasegawa, A., 2003. Repeating earthquakes and interplate aseismic slip in the northeastern Japan subduction zone, *J. geophys. Res.*, **108**(B5), 2249.
- Jepson, T.N., Bradbury, K.K. & Evans, J.P., 2010. Geophysical properties within the San Andreas fault zone at the San Andreas fault observatory at depth and their relationships to rock properties and fault zone structure, *J. geophys. Res.*, **115**(B12).
- Jolivet, R., Simons, M., Agram, P.S., Duputel, Z. & Shen, Z.-K., 2015. Aseismic slip and seismogenic coupling along the central San Andreas Fault, *Geophys. Res. Lett.*, **42**(2), 297–306.
- Kato, N., 2004. Interaction of slip on asperities: numerical simulation of seismic cycles on a two-dimensional planar fault with nonuniform frictional property, *J. geophys. Res.*, **109**, B12306, doi:10.1029/2004JB003001.
- Kato, N., 2012. Dependence of earthquake stress drop on critical slip-weakening distance, *J. geophys. Res.*, **117**, B01301.
- Kato, N. & Hirasawa, T., 1997. A numerical study on seismic coupling along subduction zones using a laboratory-derived friction law, *Phys. Earth planet Inter.*, **102**(1-2), 51–68.
- Kato, N. & Tullis, T.E., 2001. A composite rate- and state-dependent law for rock friction, *Geophys. Res. Lett.*, **28**(6), 1103–1106.
- Keilis-Borok, V., 1959. On estimation of the displacement in an earthquake source and of source dimensions, *Annali di geofisica*, **12**, 205–214.
- Lapusta, N. & Liu, Y., 2009. Three-dimensional boundary integral modeling of spontaneous earthquake sequences and aseismic slip, *J. geophys. Res.*, **114**, B09303, doi:10.1029/2008JB005934.
- Lapusta, N. & Rice, J.R., 2003. Nucleation and early seismic propagation of small and large events in a crustal earthquake model, *J. geophys. Res.*, **108**(B4), 2205.
- Lisowski, M. & Prescott, W.H., 1981. Short-range distance measurements along the San Andreas fault system in central California, 1975 to 1979, *Bull. seism. Soc. Am.*, **71**(5), 1607–1624.
- Lui, S.K. & Lapusta, N., 2016. Repeating microearthquake sequences interact predominantly through postseismic slip, *Nat. Commun.*, **7**, 13020.
- Lui, S.K. & Lapusta, N., 2018. Modeling high stress drops, scaling, interaction, and irregularity of repeating earthquake sequences near Parkfield, *J. geophys. Res.*, **123**(12), 10–854.
- Marone, C., 1998. Laboratory-derived friction laws and their application to seismic faulting, *Annu. Rev. Earth Planet. Sci.*, **26**, 643–696.
- Mitsui, Y. & Hirahara, K., 2011. Fault instability on a finite and planar fault related to early phase of nucleation, *J. geophys. Res.*, **116**, B06301, doi:10.1029/2010JB007974.
- Murray, J.R., Segall, P., Cervelli, P., Prescott, W. & Svarc, J., 2001. Inversion of GPS data for spatially variable slip-rate on the San Andreas Fault near Parkfield, CA, *Geophys. Res. Lett.*, **28**(2), 359–362.
- Nadeau, R.M. & Johnson, L.R., 1998. Seismological studies at Parkfield VI: moment release rates and estimates of source parameters for small repeating earthquakes, *Bull. seism. Soc. Am.*, **88**(3), 790–814.
- Noda, H. & Lapusta, N., 2010. Three-dimensional earthquake sequence simulations with evolving temperature and pore pressure due to shear heating: effect of heterogeneous hydraulic diffusivity, *J. geophys. Res.*, **115**, B12314, doi:10.1029/2010JB007780.
- Peng, Z., Vidale, J.E., Marone, C. & Rubin, A., 2005. Systematic variations in recurrence interval and moment of repeating aftershocks, *Geophys. Res. Lett.*, **32**, L15301, doi:10.1029/2005GL022626.
- Rice, J.R., 1993. Spatio-temporal complexity of slip on a fault, *J. geophys. Res.*, **98**, 9885–9907.
- Rice, J.R. & Ruina, A.L., 1983. Stability of steady frictional slipping, *J. Appl. Mech.*, **50**, 343–349.
- Rubin, A.M. & Ampuero, J.-P., 2005. Earthquake nucleation on (aging) rate and state faults, *J. geophys. Res.*, **110**, B11312, doi:10.1029/2005JB003686.
- Ruina, A., 1983. Slip instability and state variable friction laws, *J. geophys. Res.*, **88**(B12), 10359–10370.
- Sagy, A., Brodsky, E.E. & Axen, G.J., 2007. Evolution of fault-surface roughness with slip, *Geology*, **35**, 283–286.
- Sammis, C.G. & Rice, J.R., 2001. Repeating earthquakes as low-stress-drop events at a border between locked and creeping fault patches, *Bull. seism. Soc. Am.*, **91**(3), 532–537.
- Schaff, D.P., Beroza, G.C. & Shaw, B.E., 1998. Postseismic response of repeating aftershocks, *Geophys. Res. Lett.*, **25**(24), 4549–4552.
- Segall, P. & Rice, J.R., 1995. Dilatancy, compaction, and slip instability of a fluid-infiltrated fault, *J. geophys. Res.*, **100**(B11), 22155–22171.
- Segall, P., Rubin, A.M., Bradley, A.M. & Rice, J.R., 2010. Dilatant strengthening as a mechanism for slow slip events, *J. geophys. Res.*, **115**(B12).
- Thomas, M.Y., Lapusta, N., Noda, H. & Avouac, J.-P., 2014. Quasi-dynamic versus fully dynamic simulations of earthquakes and aseismic slip with and without enhanced coseismic weakening, *J. geophys. Res.*, **119**(3), 1986–2004.
- Titus, S.J., DeMets, C. & Tikoff, B., 2006. Thirty-five-year creep rates for the creeping segment of the San Andreas fault and the effects of the 2004 Parkfield earthquake: constraints from alignment arrays, continuous

- global positioning system, and creepmeters, *Bull. seism. Soc. Am.*, **96**(4B), S250–S268.
- Veedu, D.M. & Barbot, S., 2016. The parkfield tremors reveal slow and fast ruptures on the same asperity, *Nature*, **532**(7599), 361.
- Vidale, J.E., Ellsworth, W.L., Cole, A. & Marone, C., 1994. Variations in rupture process with recurrence interval in a repeated small earthquake, *Nature*, **368**, 624–626.
- Wu, Y. & Chen, X., 2014. The scale-dependent slip pattern for a uniform fault model obeying the rate and state-dependent friction law, *J. geophys. Res.*, **119**, 4890–4906.
- Zoback, M., Hickman, S. & Ellsworth, W., 2010. Scientific drilling into the San Andreas fault zone, *EOS, Trans. Am. geophys. Un.*, **91**(22), 197–199.
- Zoback, M. *et al.*, 2011. Scientific drilling into the San Andreas Fault zone—an overview of SAFOD’s first five years, *Sci. Drilling*, **11**, 14–28.